2D laboratory studies on Protection Measures for LWD

Wave transmission at porous breakwaters on a mangrove foreshore and

Large-scale near-shore sandbank nourishment

HCM, November 2017

LMDCZ project: Shoreline Protection Measures (WP6)

Date:	November 2017	
Document title:	2D laboratory study on protection measures for LWD	
Status:	Final	
Issued by:	Southern Water Resources Research Institute (SIWRR)	
Main authors:	Thieu Quang Tuan	
	Dinh Cong San	
	Dano Roelvink	
	Holger Schüttrumpf	
Checked by:		

Content

ACRONYMS AND SYMBOLS

LMD	Lower Mekong Delta
SIWRR	Southern Institute of Water Resources Research
CD	Chart datum (m)
WG	Wave gauge
B	Breakwater crest width, sandbank crest width (m)
D	Foreshore water depth (m)
R_c	Crest freeboard (m)
R_c/H_{m0}	Relative crest freeboard (-)
B/H_{m0}	Relative crest width (-)
SWL	Still water level (m)
N_L	Model length scale (-)
N_t	Model time scale (-)
N_w	Model sediment fall speed scale (-)
H_{m0}	Zero-th moment spectral wave height (m)
$T_{m-1,0}$	Characteristic spectral wave period
K_t	Wave transmission coefficient (-)
K_{re}	Wave reduction coefficient (-)
R	Wave reflection coefficient
f	Wave frequency
S(f)	Variance density (m2/Hz)
f_{min}	Minimum frequency considered
f_{max}	Maxiumum frequency considered
m_n	n^{-th} spectral moment
IG	Infragravity

1 Introduction

a. Background

The mangrove-mud coast of the Lower Mekong Delta (LMD) has been suffering from severe erosion over the past few decades. Sediment imbalances at various temporal and spatial scales induced by both human activities and nature are the main cause of the erosion.

The study area of LWD is split into several sub-areas, in which soft and/or hard protective measures have appropriately been proposed in accordance with their natural conditions, the cause of erosion and priority/projection for social and economic development.

Hard measures - Detached porous breakwater

A proposed hard protective measure is considered appropriate only if it enhances local sediment balances and thus accommodates mangrove rehabilitation efforts. The applied structure should function like mangrove plants as much as possible, i.e. tide and sediment exchange, wave absorption, and efficient sediment entrapment. Besides, it should be structurally stable against design wave attack and able to withstand on a soft mud foundation of LWD.

Figure 1 Pilot project of porous detached breakwater at Long Hai beach (Ba Ria Vung Tau province)

Detached (shore-parallel) breakwaters of porous elements as illustrated in Fig.1 are considered an applicable protective measure against beach erosion. This is a type of porous (hollows take up about 20% surface area) and narrow-crested structure. The idea is that the structure is sufficiently permeable so tide with fine sediment can go through and is high enough to dissipate wave

energy, consequently promoting onshore sedimentation.

A pilot construction has been executed at Long Hai beach (see Fig.1). Though this was done without appropriate understanding of the structure functionality the structure has shown its high efficiency in damping waves and promoting sedimentation. However, to achieve the ultimate goal of coastal protection aspects of functional design of the structure must be realized at the first design stage. In essence, wave damping capacity, wave reflection and sediment entrapping efficiency are necessary for this design purpose.

In this study the main focus is on wave transmission and reflection at this type of porous breakwater. In a 2D situation (wave flume) sediment in suspension is proportional to the wave height and wave damping capacity also reflects sediment trapping efficiency of the structure, tests on sediment trapping are therefore disregarded herein. Tests with muddy water or dye shall be carried out latter to demonstrate if the sediment exchange (or transport of sediment) through the breakwater is possible.

In the literature there exist numerous studies on wave transmission at conventional types of structures such as rubble-mound breakwaters, smooth and impermeable breakwaters, etc. (see e.g. van der Meer et al., 2005). However, these mostly concern with structures in relatively deep water, probably inapplicable for those with porous bodies and on very shallow foreshores considered herein. Due to drastic spectral transformation by depth-induced wave breaking, the incoming wave may interact differently with the structure, resulting in a noticeably different wave transmission (see Tuan et al., 2016).

For the purpose of functional design, it is therefore required at first a quantitative understanding of wave transmission in this special circumstance. Measured laboratory data are used to derive a new empirical formulation of wave transmission at the porous breakwater on a mangrove foreshore. The result shall also be compared with some existing formulations of conventional structures.

Soft measures – Large-scale nourishment by near-shore sandbanks

Besides hard alternatives, soft measures following the strategy of “building with nature”, which makes use of natural processes to provide protection services for the coast and/or to support mangrove rehabilitation efforts, must be given a priority wherever possible. In this context, bamboo fences and large-scale nourishment by near-shore sandbanks are considered applicable for a mangrove-mud coast. Within the scope of this laboratory study, only the latter is considered.

The idea behind the large-scale nourishment is to have a wide and segmented system of sandbanks at a distance from the shore, mimicking natural submerged sandbars. A system of sandbanks is designed in such a way that it would significantly reduce the wave energy and still allow mud to be exchanged between near-shore shelf and mangroves and to be transported alongshore. Sandbanks gradually deform due to alongshore and cross-shore transport processes but simultaneously feed the coast and thus would have to be replenished at certain intervals.

Because the wide-crested sandbank is like a submerged reef and the aforementioned special wave characteristics on the shallow mangrove foreshore, the wave hydrodynamics across sandbanks is rather unique. For the functional design of the nourishment, it is of interest to investigate the effect of sandbank on the near-shore wave hydrodynamics, i.e. wave transmission and spectral transformation. Moreover, the extent of sandbank profile response induced by cross-shore processes under various wave and water level conditions hints at the nourishment efficiency.

b. Aims and scope

In summary, scale model experiments carried out at River and Marine Hydrodynamic Laboratory of SIWRR have the following aims:

- To increase understanding of cross-shore physical processes involved, needed for the functional design purposes
  - Detached porous breakwater: wave transmission, reflection
  - Nourishment by sandbanks: wave transmission, spectral transformation and profile response
- To generate data for numerical validations.

Note that all experiments were carried out in a wave flume, which address across-shore processes only. Also, aspects of structural design during extreme events: wave loading, stability, etc. are beyond the scope of this study report.

This report is organized as follows. The model setup and test program and experimental results for each of the tested protective measures, viz. wave transmission at porous breakwaters and the large-scale nourishment, are discussed in Section 2 and Section 3, respectively.

2 Wave transmission and sediment exchange at porous breakwaters

a. Model setup and test program

The experiments were carried out in the wave flume at River and Marine Hydrodynamic laboratory of Southern Water Resource Academy (Binh Duong province, Vietnam). The facilities were constructed with all the equipment installed by HR Wallingford in 2014. The flume is 35 m long (effective), 1.2 m wide and 1.5 m high, equipped with an automated system of Active Reflection Compensation (ARC) and capable of generating both regular and irregular waves up to 0.3 m in height and 3.0 s in peak period. Reliable resistance-type wave gauges are available for measuring wave signals at sampling frequency up to 100 Hz (accuracy $\pm$ 0.1 mm).

Figure 2 illustrates the model setup for experiments. The model breakwater, 0.4m high, is founded on a mangrove foreshore with slope of 1/500. A transitional segment with slope of 1/25 is introduced between the gentle foreshore and the deep water section so that waves are well

generated at the offshore boundary. Moreover, incoming waves are forced to break around the slope transition, creating wave breaking condition on the foreshore similar to that in the field. To effectively absorb the remaining wave energy, a gentle rock slope (slope 1/4) as a passive wave absorber is placed at the other end of the flume. Calibration tests without the structure show that the reflection coefficient was always less than 10%.

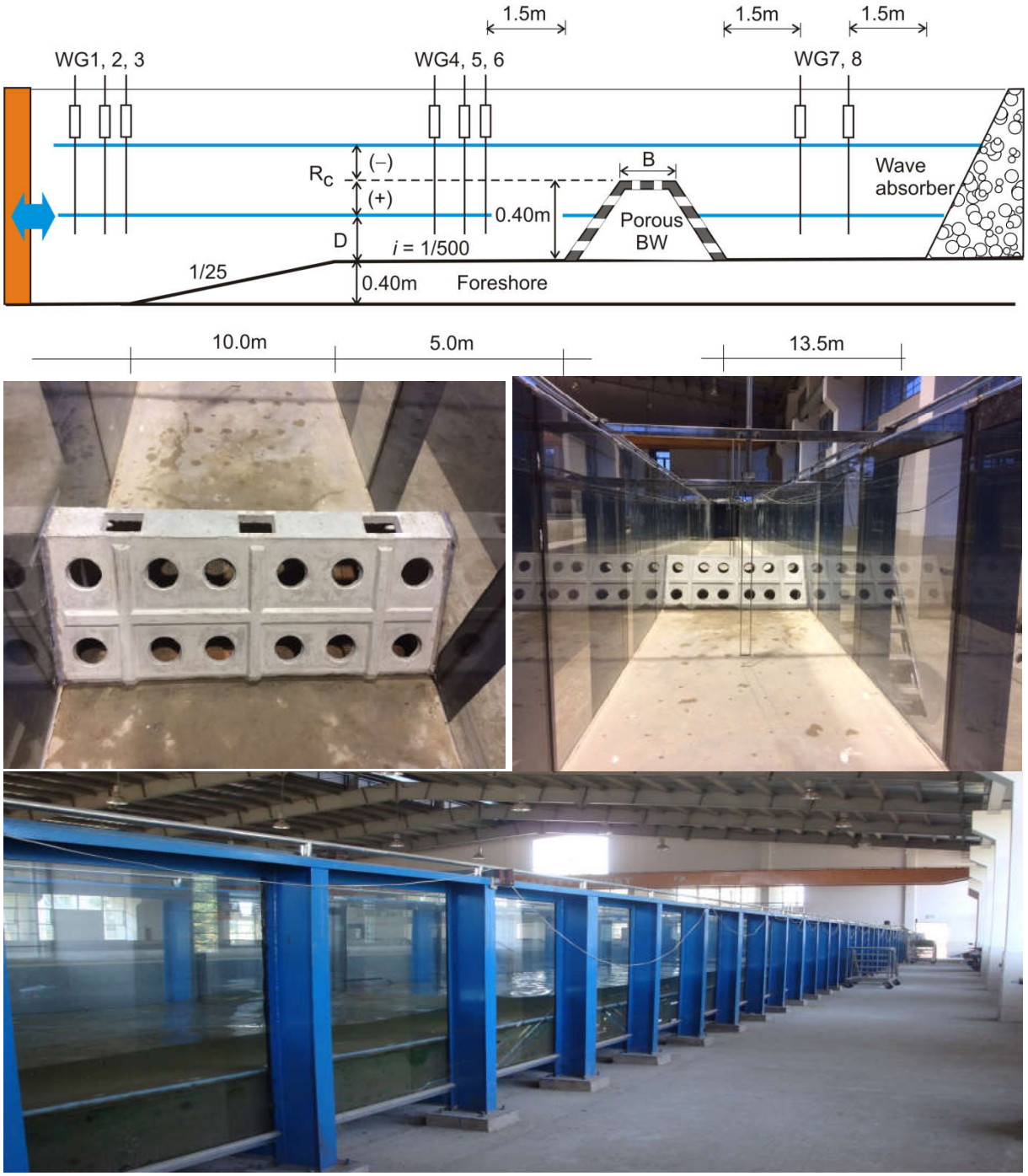

Figure 2 Model setup of wave transmission at porous breakwaters

Wave parameters in font and behind the breakwater were measured with eight capacitance wave gauges. Incident and reflected waves were separated according to the approach by Zelt and Skjelbreia (1992) using the first three-gauge array at the inflow boundary. A Hanning window was used for visualization of calculated wave spectra. A cut-off frequency of 0.025 Hz was also applied to exclude the energy part of the resonance frequency of the flume. The analysis of wave transmission involves the following parameters derived from the measured wave data.

Spectral wave height H_{m0}:

$$H_{m0} = 4{,}004\ \sqrt{m_0} = 4{,}004\ \sqrt{\int_{f\min}^{f\max} S(f)df} \tag{1}$$

where m_0 is spectral zero^{-th} moment, $S(f)$ is spectral variance density.

Besides the peak spectral period T_p, characteristic spectral period $T_{m-1,0}$ is also determined for cases of flatten wave spectra in shallow water.

$$T_{m-1,0} = \frac{m_{-1}}{m_0} = \frac{\int_{f\min}^{f\max} f^{-1}S(f)df}{\int_{f\min}^{f\max} S(f)df} \tag{2}$$

Having known the wave heights in front of and behind the structure the wave transmission coefficient can be determined accordingly (see also Fig. 3):

$$K_t = \frac{H_{m0,t}}{H_{m0,i}} \tag{3}$$

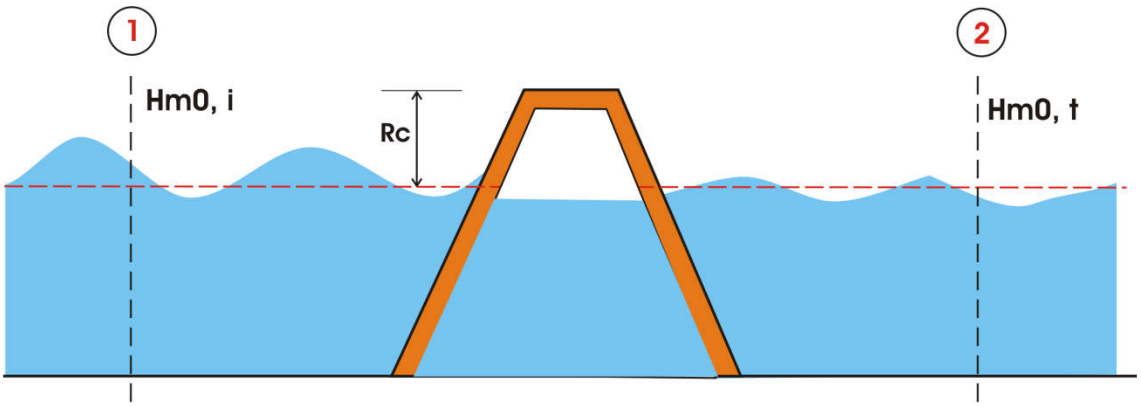

Figure 3 Definition sketch of wave transmission and wave reduction coefficients

where K_t is transmission coefficient, $H_{m0,i}$ and $H_{m0,t}$ are the incident (location 1 in Fig.3) the transmitted wave height (location 2 in Fig.3), respectively.

Alternatively, the wave damping capacity of the structure can also be evaluated via a wave reduction coefficient due to the presence of the structure:

$$K_{re} = \frac{H_{m0,bef}}{H_{m0,aft}} \tag{4}$$

where K_{re} is wave reduction coefficient, $H_{m0,bef}$ and $H_{m0,aft}$ are wave heights at a given location before and after the presence of the structure (such as location 2 in Fig.3), respectively.

The testing program as summarized in Table 1 consists of 60 test scenarios (including 30 base or no structure scenarios), resulting from 06 typical monsoon waves in combination with 05 water levels (both emerged and submerged) derived from typical hydraulic conditions of LWD. Note that the typical height-period relation of monsoon waves is according to Linh and Tuan (2015).

Since no measured wave spectrum on the mangrove foreshore (shallow water) is available, standard JONSWAP spectra with γ = 3.30 were used for generation of tested waves at the offshore boundary. Each of the experiments lasted approximately 500.T_p to adequately produce the main frequency domain of desired wave spectra.

The scaling law for wave transmission is basically according to Froude's criteria, whereby the time scale N_t can be derived in connection with the length scale N_L.

$$N_t = N_L^{0.5} \tag{5}$$

The chosen length scale is N_L = 10 (N_t = 3.16), based on the flume capacity and the tested range of hydraulic parameters.

Table 1 A summary of test program on wave transmission

Test waves (Offshore boundary)	**Target values**		**Freeboard Rc/ Depth D (m)**	**Model breakwaters**
	H_{m0} (m)	**T_p (s)**		
WP6-BW-JSW1	0.10	1.79		
WP6-BW-JSW2	0.12	1.88	0.20/0.20	
WP6-BW-JSW3	0.15	2.00	0.10/0.30	No breakwater
			0.00/0.40	
WP6-BW-JSW4	0.17	2.07	−0.10/0.50	Porous breakwater
WP6-BW-JSW5	0.20	2.16	−0.15/0.55	
WP6-BW-JSW6	0.22	2.20		

b. Data analysis and results

Influencing parameters on wave transmission

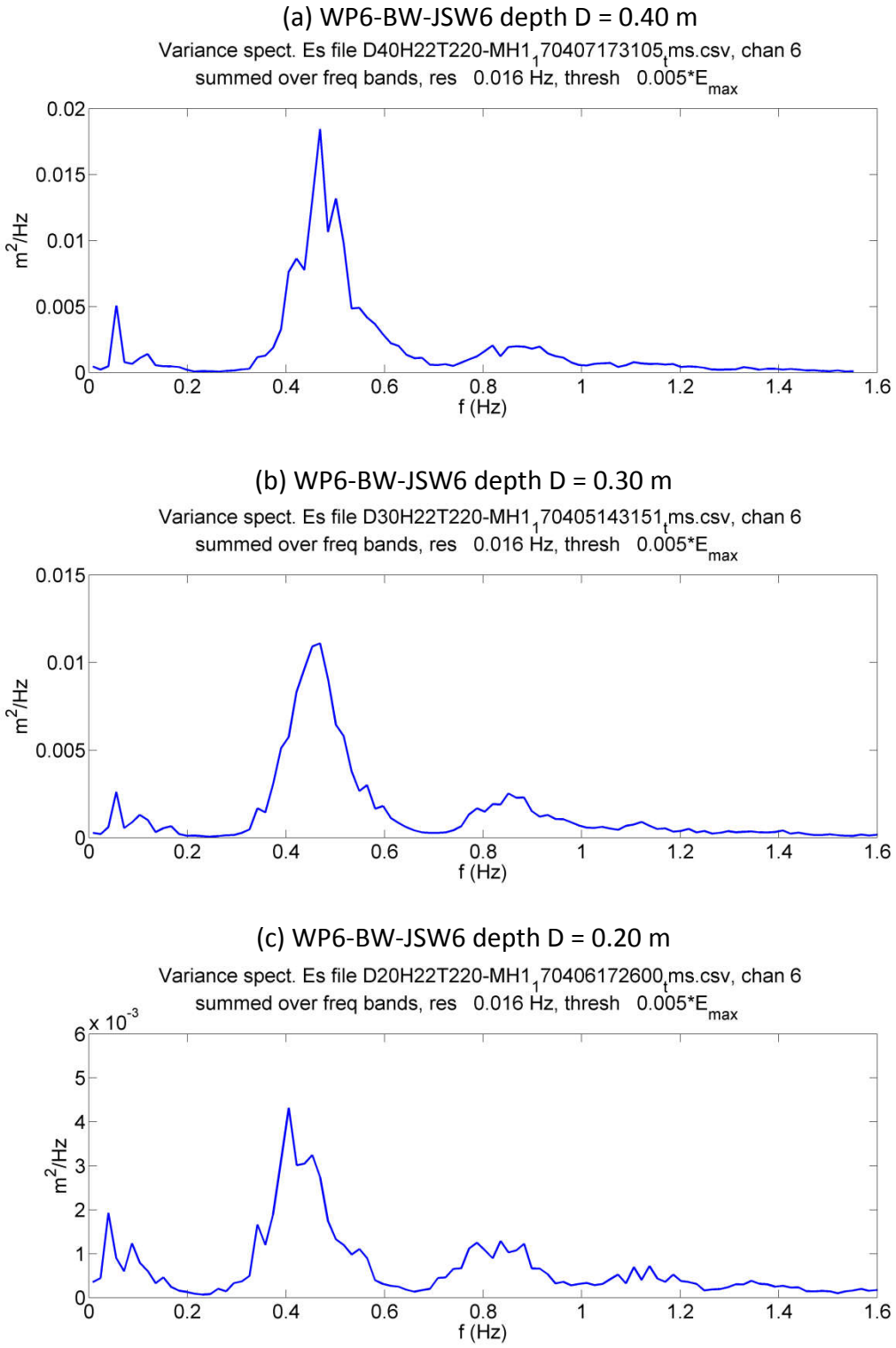

Figure 4 Measured shallow wave energy spectra at WG6 on the foreshore (wave WP6-BW-JSW6)

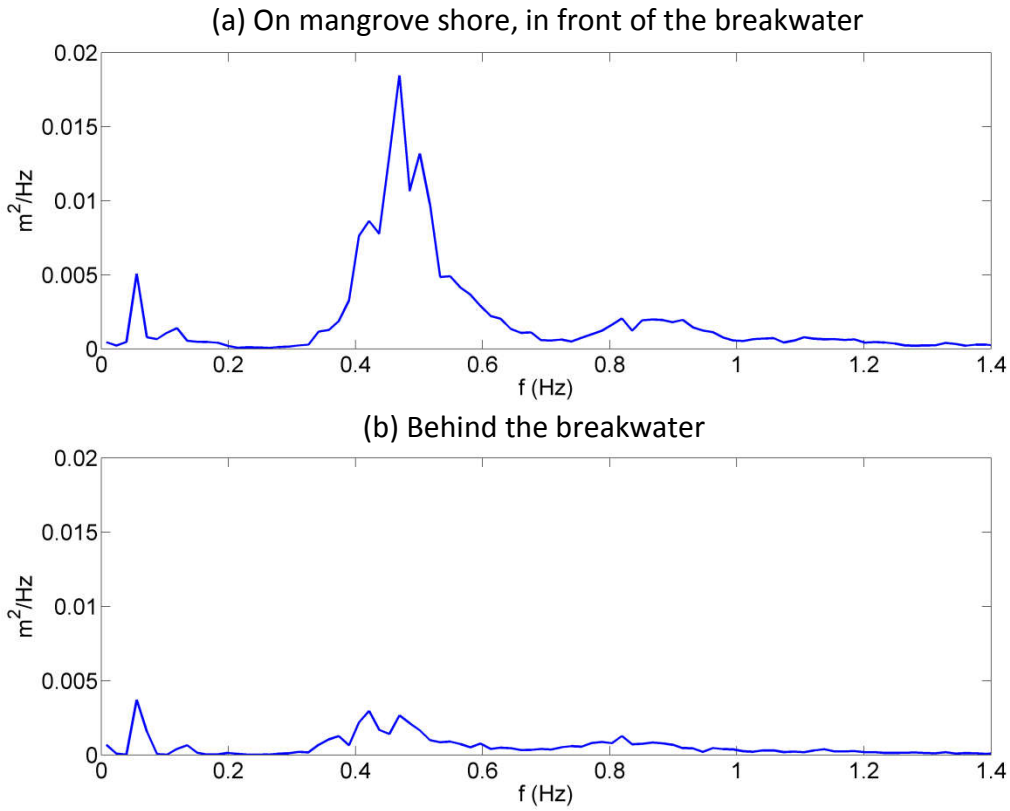

Figure 5 Wave energy spectra across the breakwater (test WP6-BW-JSW6-D40)

Like other conventional breakwaters, wave transmission at porous breakwaters is generally a function of relative crest freeboard, crest width, breakwater slope, porosity/permeability, and wave characteristics. In order to arrive at an empirical formulation for wave transmission, effects on wave transmission of most influencing parameters like the relative crest freeboard and Iribarren number are analyzed with the experimental data. Other secondary parameters such as the crest width (porous breakwaters are a narrow-crested structure) and porosity, for the type of structure being considered herein, are implicitly included and thus are not present in the analysis.

Wave spectral transformation in shallow water

At first we examine the behaviour of wave spectral transformation on the foreshore and across the breakwater. Measured wave spectra as shown in Fig. 4 at a location on the foreshore (WG6) clearly exhibit multiple peaks and flatten as wave breaking increases. Noticeably, low frequency or infragravity waves (hereafter designated as IG waves, period of around 25 s herein) are present and generated by the breaking processes of short-period waves on the steep transitional slope and on the shallow foreshore (i.e. moving breakpoint of short-period waves, see e.g. Baldock, 2012). Alternatively, forced bound long waves induced by wave grouping are also released as free IG waves at breaking points of gravity waves. The existence of these IG waves is probably inherent to the wave dynamics on a shallow mangrove foreshore, similar to that on a shallow fringing reef.

As short (gravity) waves break the relative importance of IG waves start to increase.

Consequently, the long wave energy can take up a major part of the total wave energy in the surfzone of a mangrove foreshore (see e.g. Horstma et al., 2012; Phan et al., 2014). This also applies for wave transmission considered herein. Figure 5 illustrates the spectral transformation across the breakwater with a high crest emergence, showing short-wave energy largely dissipates (and filtered out) whilst long-wave energy still remains at large.

The above observation of spectral transformation underlies the importance of long waves in wave transmission at coastal structures in the surfzone of a mangrove foreshore. The spectral peak period appears not to be representative for multi-peak spectra, inquiring the use of a more appropriate characteristic wave period in describing wave transmission on a shallow foreshore. As hint at from wave overtopping the spectral period $T_{m-1,0}$, which gives more emphasis on the contribution of long waves in shallow water, would also be a good choice.

Relative crest freeboard R_c/H_{m0}

The relative crest freeboard R_c/H_{m0} always plays the most important role in wave transmission at coastal structures. Without exception, Fig. 6 shows a strong dependency of the wave transmission coefficient K_t (blue points, Eq. (3)) and the wave reduction coefficient K_{re} (red points, Eq. (4)) on the crest freeboard. It follows that the transmission coefficient quickly declines in a linear trend with the increase of the relative freeboard and becomes almost constant (K_t ~ 0,30) when R_c/H_{m0} > 0.50. Generally speaking, wave is not much transmitted through the breakwater with high crest emergence. On the other hand, the structure is not effective in damping wave when it gets submerged, i.e. $K_t = 0.75 - 0.80$ as $R_c/H_{m0} < -0.50$.

Note that hereinafter wave transmission coefficient K_t according to Eq. (3) shall be used in the analysis.

Reference is made to Annex A for more details on the experimental data.

Iribarren number ξ_0

Wave transmission also depends the behaviour of waves on the breakwater slope or the wave-structure interaction expressed via the Irribarren number ξ_0. Figure 7 describes dependency of ξ_0 derived from the experimental data with both the peak period T_p (ξ_{0p}) and the spectral period $T_{m-1,0}$ ($\xi_{0m-1,0}$). In general, the dependency of ξ_0 follows a nonlinear (or exponential) trend and is rather weak for both high and low R_c/H_{m0} (not shown in Fig. 7). Clearly, the correlation appears to be better with the use of $T_{m-1,0}$ than that with T_p.

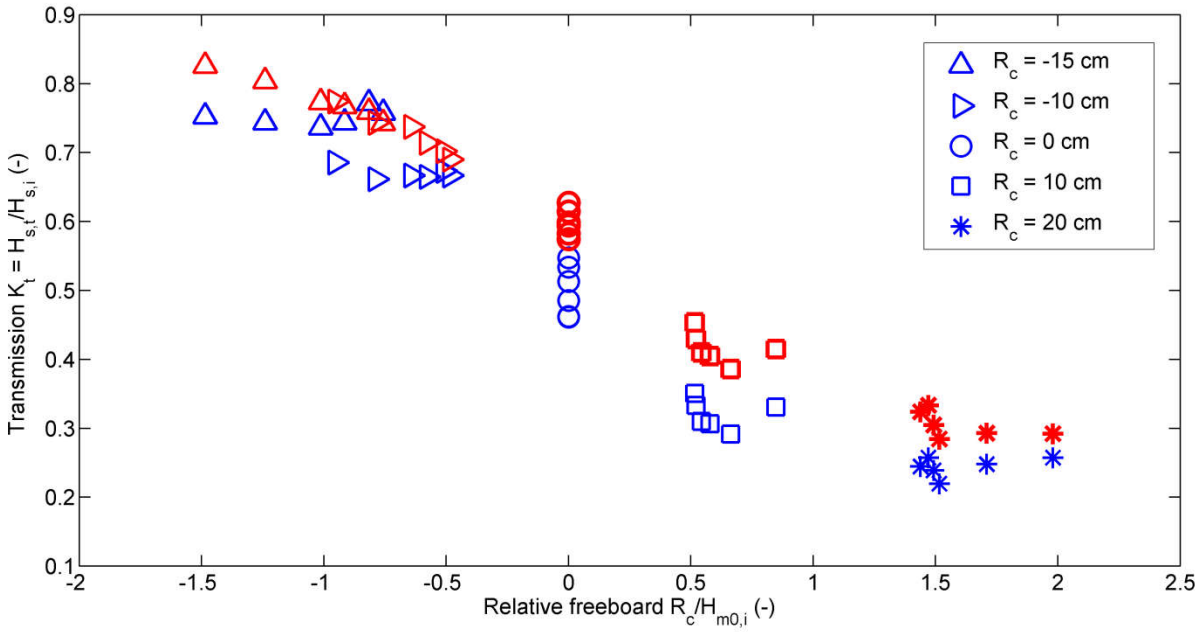

Figure 6 Effects of relative crest freeboard on wave transmission

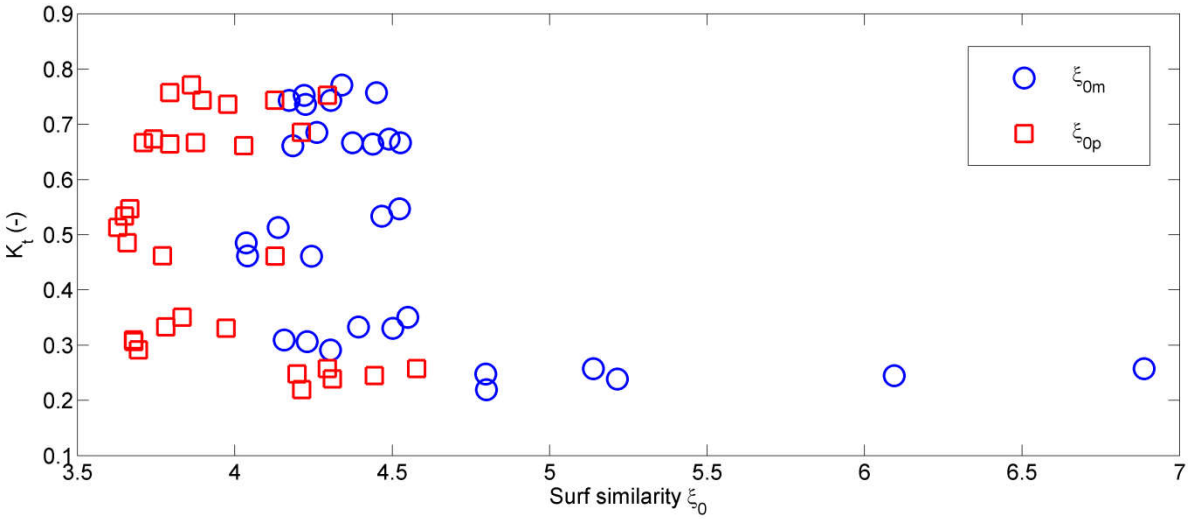

Figure 7 Dependency of Iribarren number ξ_0

Reflection

Wave reflection at a structure is a response as the result of wave-structure interaction. Though reflection is not explicitly described in wave transmission, it hints at the efficiency of energy dissipation of a structure.

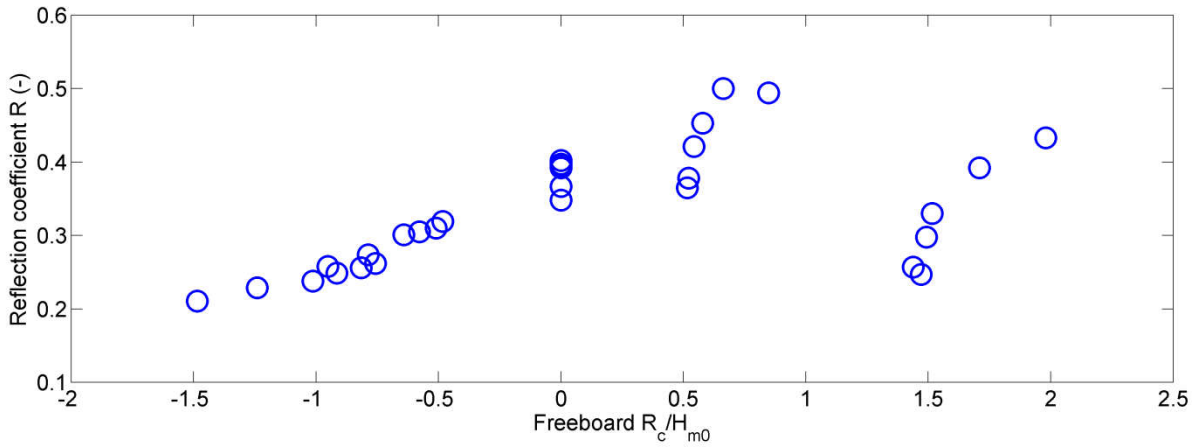

Figure 8 Reflection coefficient as a function of R_c/H_{m0}

The reflection coefficient plotted against the relative freeboard in Fig.8 indicates that the porous breakwater is highly reflective, particularly when the crest emerges above water (R = 0.40 ~ 0.50). Reflection generally increases with the increase of R_c/H_{m0}. This is because the structure is not sufficiently porous to absorb wave energy and so, in case of high crest emergence, most of the wave energy behind the breakwater is actually from transmitted IG waves and wake of wave overtopping.

It is important to realize this high reflection character in the structural design of porous breakwaters, especially care must be taken in the design of toe scour protection.

Empirical formulations of wave transmission

The above analysis on parameters that most influence wave transmission forms the basis for derivation of an empirical formulation. The influence of the governing parameters suggests that a similar form of the formulation by Angremond et al. (1996) can be used to derive the empirical formula for wave transmission herein. The two main considered variables are relative crest submergence R_c/H_{m0} and Iribarren number ξ_0. A general formulation of wave transmission at porous breakwaters can be expressed as follows:

$$K_t = a \cdot \frac{R_c}{H_{s,i}} + b \cdot \left(1 - e^{-c \cdot \xi_0}\right) \tag{6}$$

in which a, b, and c are empirical constants determined through regression analysis with the experimental data.

Note that compared to Angremond et al. (1996) the crest width B is not present in Eq. (6) since the porous breakwater is considered a narrow-crested type of structure (in fact its effect is implicitly included). Also, the Iribarren number ξ_0 can be determined either with T_p or $T_{m-1,0}$, depending on their availability.

Regression analysis with the experimental data results in the following two formulations of wave transmission with ξ_0 according to $T_{m-1,0}$ and T_p, respectively:

$$K_t = -0.22 \cdot \frac{R_c}{H_{s,i}} + 0.75 \cdot \left(1 - e^{-0.26 \xi_{0m-1,0}}\right) \tag{7}$$

$$K_t = -0.20 \cdot \frac{R_c}{H_{s,i}} + 0.66 \cdot \left(1 - e^{-0.39 \xi_{0p}}\right) \tag{8}$$

The above formulations are valid within the tested range of governing parameters:

$$\begin{aligned} &\frac{R_c}{H_{m0}} = -0.76 \sim 2.0 \\ &s_{0p} = 0.016 \sim 0.030 \\ &s_{0m} = 0.010 \sim 0.025 \\ &K_t = 0.22 \sim 0.77 \end{aligned} \tag{9}$$

Figures 9 and 10 compare the calculated K_t according to Eq. (7) and (8) with the measured data, respectively. Agreement is generally good for both cases and slightly better with the use of $T_{m-1,0}$.

Cross-comparisons of the present study, as shown in Figs. 11 through 13, with existing formulations by d'Angremond et al. (1996) and van der Meer et al. (2005) for smooth and impermeable breakwaters, van der Meer et al. (2005) for rough and permeable breakwaters, and van der Meer and Daemen (1994) for narrow-crested, rough and permeable breakwaters were also made, respectively. It follows that except a satisfactory agreement is found with the formulation by van der Meer et al. (1993) for narrow-crested permeable structures, all other slightly to largely overestimate the transmission coefficient. This is in part due to the foreshore influence on the spectral transformation of the incoming wave mentioned earlier. Also, the porous breakwater considered herein appears to be closer to the type of narrow-crested, rough and permeable structure.

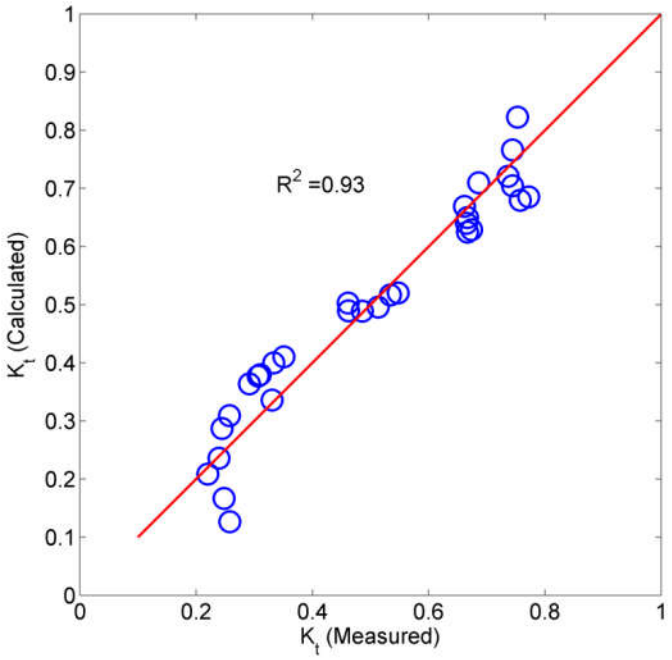

Figure 9 Data regression with $\xi_{m-1,0}$

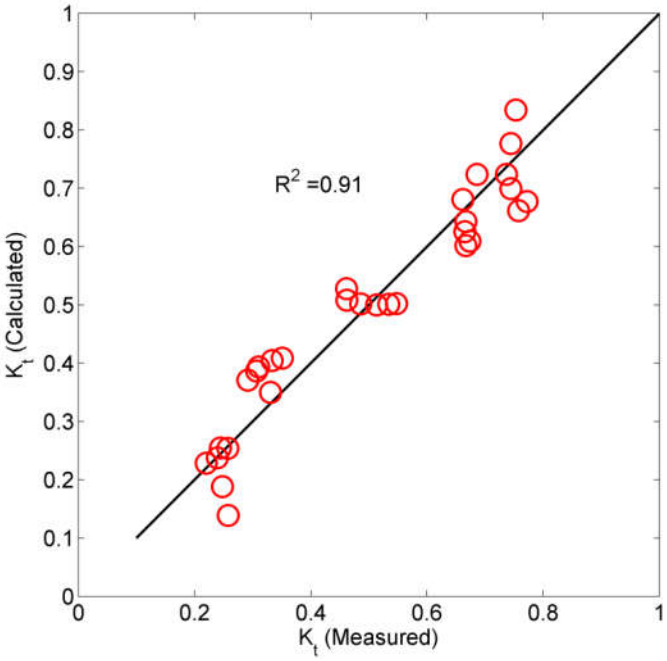

Figure 10 Data regression with ξ_{0p}

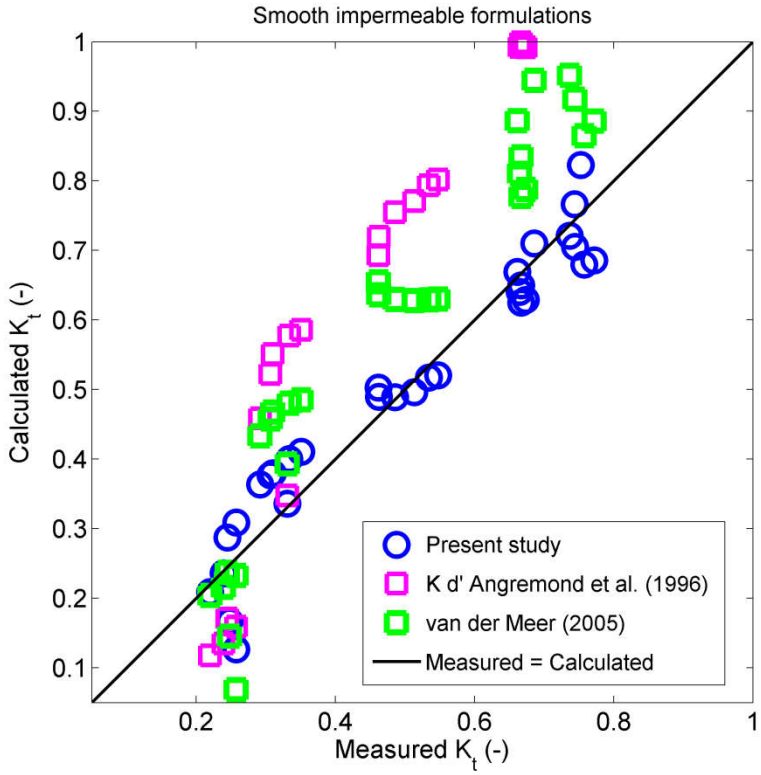

Figure 11 Comparison with formulations of smooth and impermeable breakwaters (Angremond et al., 1996 and van der Meer et al., 2005)

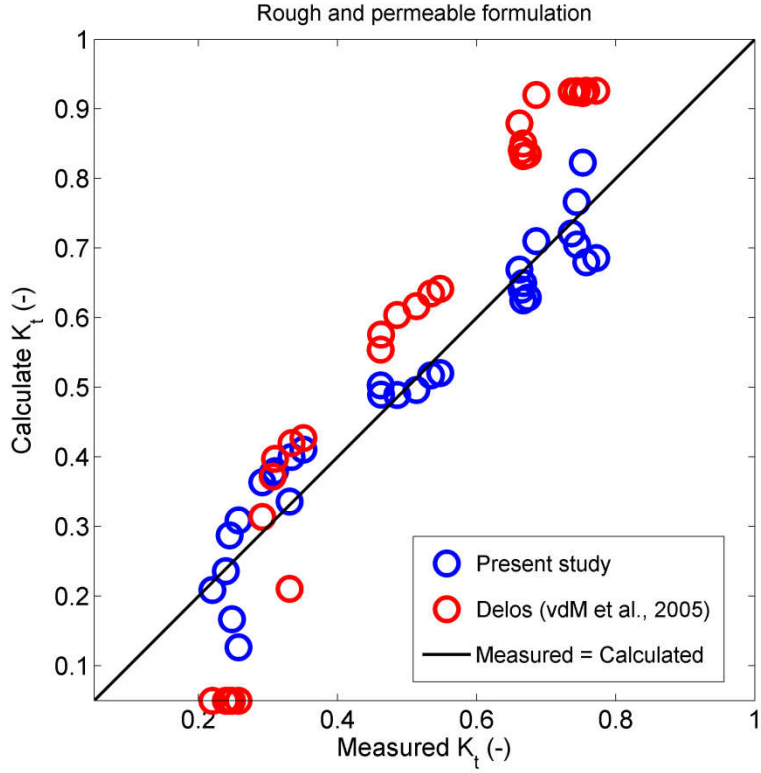

Figure 12 Comparison with formulations of rough and permeable breakwaters (DELOS - van der Meer et al., 2005)

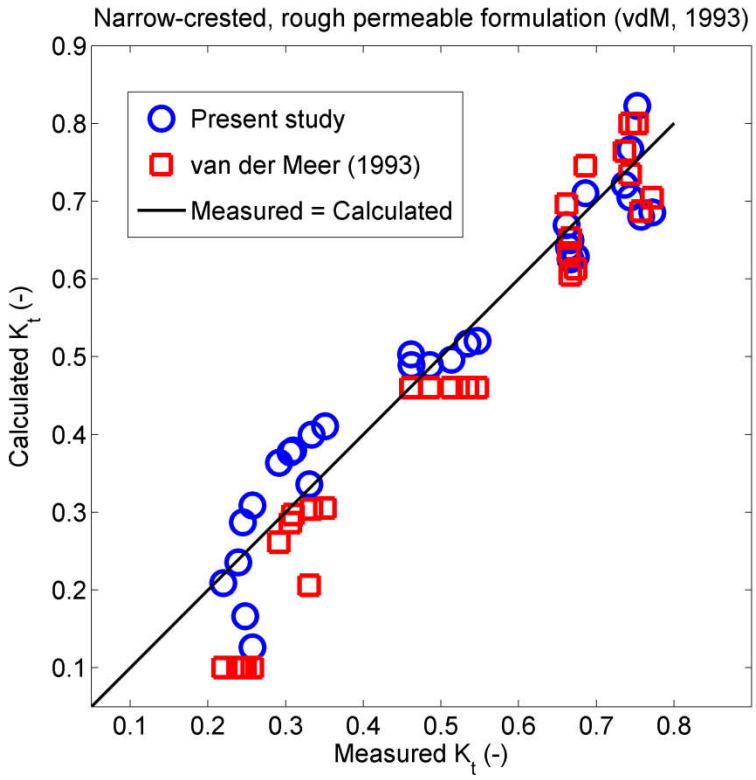

Figure 13 Comparison with formulations of narrow-crested, rough and permeable breakwaters (van der Meer and Daemen, 1994)

c. Sediment exchange capacity

Details of the experimental setup and results are addressed in a separate report.

d. Summary and Remarks on porous breakwaters

For the functional design of porous breakwaters on mangrove foreshore, a testing program consisting of 60 model experiments on wave transmission with governing parameters covering the typical range of hydraulic boundary data of LWD was carried out. Behaviour of wave spectral transformation on the shallow mangrove foreshore and across the breakwater reveals the relative importance of long-period wave energy in the wave transmission. As most short-period energy is dissipated and/or reflected back, long-period energy takes up the major part in the transmitted wave behind the breakwater.

Data analysis identifies the two most important governing variables of wave transmission at a porous breakwater which are the relative crest freeboard R_c/H_{m0} and the behaviour of waves on the dike slope expressing through Iribarren number ξ_0. The characteristic spectral period $T_{m-1,0}$ should be used instead of peak period T_p to give more emphasis on the effect of long-period waves in shallow water.

A new set of empirical formulae have been derived, allowing for a reliable determination of wave transmission at the considered porous type of breakwaters on a shallow mangrove foreshore. Cross-comparison with several existing formulations, such as by d'Angremond et al. (1996), van der Meer et al. (2005) and van der Meer and Daemen (1994) for various types of conventional breakwaters, implies that the behaviour of wave transmission considered herein is very close to that at a narrow-crested, rough and permeable breakwater.

For the purpose of functional design of porous breakwaters, it is recommended to take into account the following considerations:

- The design crest level should be above high tide (emerged structures) to be effective in damping waves. Wave is almost blocked as $R_c/H_{m0} > 0.50$.
- Because structure of this type is highly reflective, special attention must be paid to the design of toe scour protection.

Recommendations for future research include physical experiments on wave loading and structural stability so that the structure can be designed to withstand wave attack during extreme events.

3 LARGE-SCALE NOURISHMENT BY NEAR-SHORE SANDBANKS

a. Model setup and test program

Figure 14 illustrates the model setup for the experiments of nourishment. The model sandbank, placed on a shallow mangrove foreshore as used previously, has the crest width of B and is 0.20 m above the bed.

As usual, Froude and relative sediment fall speed similitude criteria are selected to satisfy as they are the major underlying physics behind the gravity-induced sediment transport processes (see e.g. Hughes, 1993). Also, it is customary to use the same sediment as in nature and the model is geometrically undistorted. These lead to the following scaling relations:

$$N_w = N_L^{0.5}$$
$$N_t = N_L^{0.5} \tag{10}$$

where N_w is the sediment fall speed scale.

The fall speed of sediment w_s can be estimated according to:

$$w_s = \frac{10\nu}{d_{50}}\left[\left(1+0.01\Delta g d_{50}^3 \nu^{-2}\right)^{0.5} - 1\right] \tag{11}$$

where ν is molecular fluid viscosity, Δ (= 1.65) is relative submerged density of sediment.

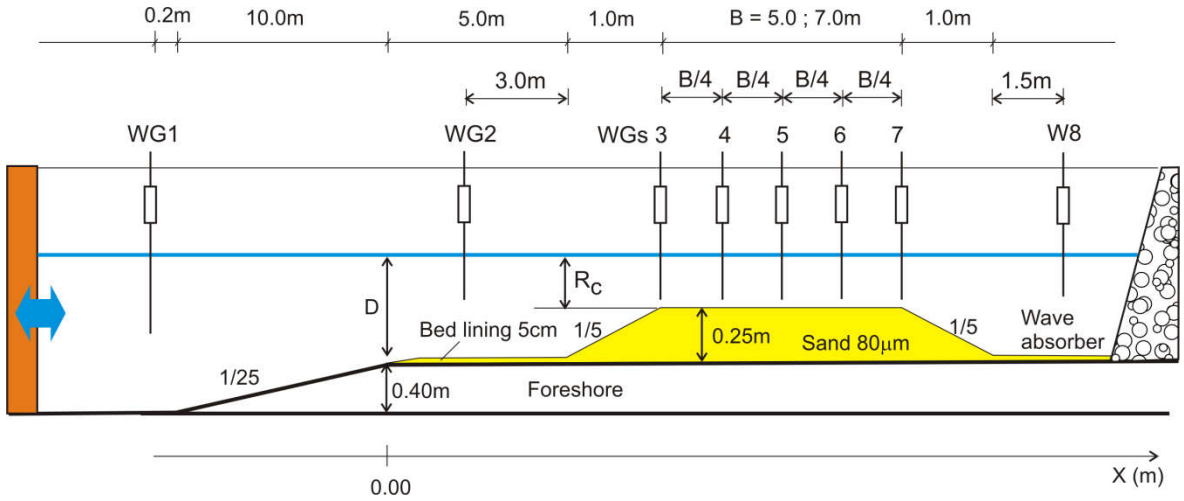

Figure 14 Test setup of nourishment by sandbanks

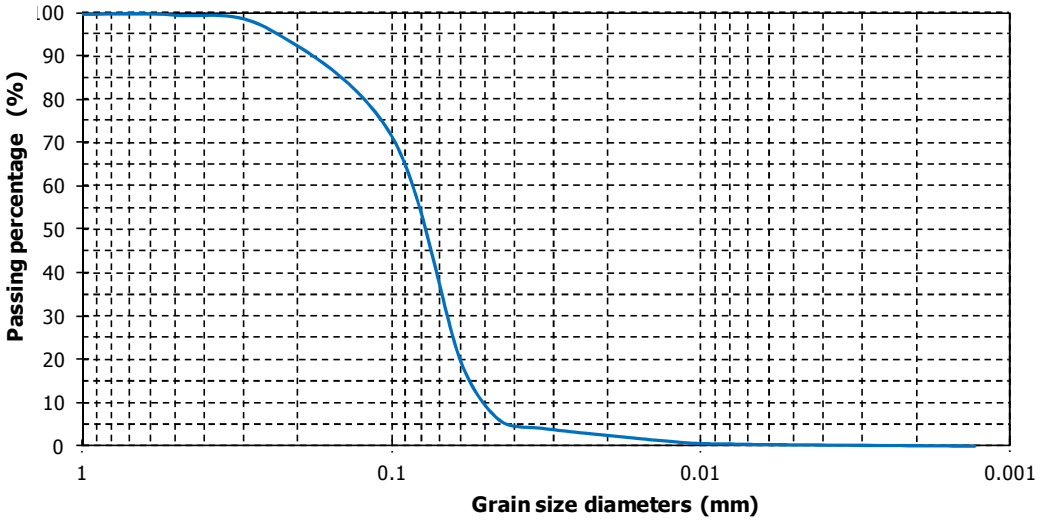

Figure 15 Grain size distribution of model quartz sand

The median size d_{50} of the model quartz sand is 80 μm (see Fig. 15) and that of most available borrow sand in study area is 200 μm, which result in a model length scale N_L of about 1/20.

Wave measurements at various locations along the longitudinal axis were used to evaluate the cross-shore spectral transformation and wave damping capacity of the sandbank. To double-check the effect of high sediment concentration on the conductivity of water and thus the recorded wave signals, all wave gauges were carefully calibrated before and after each test. Averaged calibration coefficients were taken.

Simultaneous flow measurement at several locations across the sandbank would be ideal for validation of numerical models. Unfortunately, this was not possible due to lack of equipment.

The model sandbank was rebuilt after each test and sand samples at various locations were taken for determining the sand porosity as built. The average porosity was 0.430. The pre- and post-storm sandbank profiles were averaged over 03 measuring lines (two at 10 cm away from the side walls and one at the middle of the flume) with ordinary land survey equipment. To have a rough impression on the time-dependent sandbank profile response instantaneous sandbank profiles were also marked on the glass walls and measured at several intermediate time steps. The whole progress of sandbank deformation during testing was recorded with a HD video camera viewed through the glass wall. Example photos of the experiments are shown in Fig. 16.

(a) Before testing

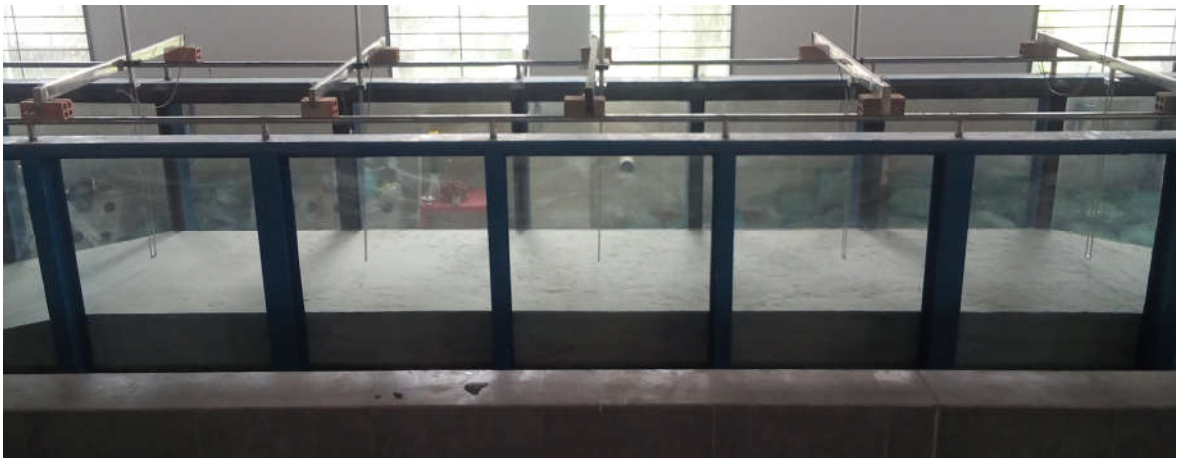

(b) During testing: severe wave breaking and high sediment concentration

(c) Sandbank deformation after testing

Figure 16 Photos of model experiments

The test program as summarized in Table 2 consists of 08 experiments, in which each of the two sandbank models (B = 5m and 7m) was tested with several (wave + water level) scenarios.

Following the design philosophy of the nourishment, the model sandbank was kept sufficiently submerged so that no major bed deformation occurred during testing whilst still maintaining a high level of wave damping. The test waves at the offshore boundary, downscaled from typical monsoon waves, were standard JONSWAP. Each test lasted between 3000 and 5000 waves, depending on the actual extent of sandbank deformation.

Table 2 Test program of the nourishment by sandbanks

Test scenarios	Model					Prototype				
	B (m)	R_c (m)	H_{m0} (m)	T_p (s)	Dura. (min.)	B (m)	R_c (m)	H_{m0} (m)	T_p (s)	Dura. (hrs.)
WP6-NOU-B5-R05-JSW1	5.0	−0.05	0.08	1.44	120	100	−1.0	1.60	6.44	8.94
WP6-NOU-B5-R15-JSW1	5.0	−0.15	0.08	1.44	75	100	−3.0	1.60	6.44	5.59
WP6-NOU-B5-R05-JSW2	5.0	−0.05	0.10	1.53	125	100	−1.0	2.00	6.84	9.32
WP6-NOU-B5-R10-JSW2	5.0	−0.10	0.10	1.53	80	100	−2.0	2.00	6.84	5.96
WP6-NOU-B5-R15-JSW2	5.0	−0.15	0.10	1.53	125	100	−3.0	2.00	6.84	9.32
WP6-NOU-B7-R10-JSW2	7.0	−0.10	0.10	1.53	125	140	−2.0	2.00	6.84	9.32
WP6-NOU-B7-R10-JSW3	7.0	−0.10	0.12	1.61	134	140	−2.0	2.40	7.20	9.99
WP6-NOU-B7-R10-JSW4	7.0	−0.10	0.14	1.69	141	140	−2.0	2.80	7.56	10.51

Note: Wave parameters are desired values at offshore boundary (WG1)

b. Data analysis and results

Spectral transformation and wave transmission

Following the same procedure of wave analysis as mentioned in Section 2.1, wave spectra at measured locations across the sandbank are determined. In a mobile bed experiment, one may wish to know the time-varying wave heights. However, it is observed herein that major bed changes mostly took place during the first 500-1000 waves (see also Section 3.2.2), after which wave regime across the bank became relatively stable. An example of time variation of wave transmission from test scenario WP6-NOU-B5-R05-JSW2 with noticeable bank deformation during the first 1000 waves (50 min.) is shown in Fig. 17. It follows that the transmitted wave height (at WG8) becomes almost constant after 50 minutes (slightly decreased as the bank crest marginally elevated by on-shore sand deposition). Therefore, for the purpose of evaluation of wave transmission discussed herein we advocate a practical and probably more appropriate approach that is to determine the wave heights once the bank profile has become relatively stable (after approximately the first 1000 waves).

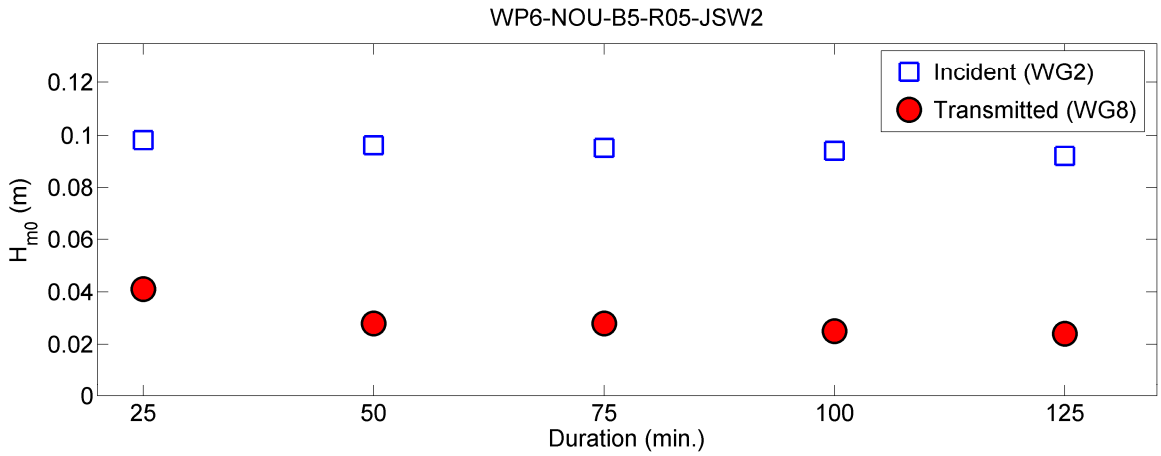

Figure 17 Time-varying wave transmission: WP6-NOU-B5-R05-JSW2

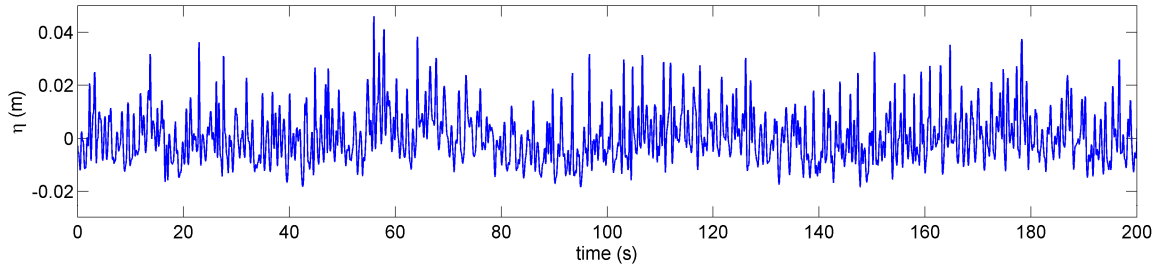

Figure 18 Wave signal with presence of IG waves: WG7- WP6-NOU-B7-R10-JSW3

The wave hydrodynamics over the sandbank resembles that over a shallow reef due to a similarity in geometrical conditions. Figure 18 shows the presence of IG waves in a recorded wave signal, an important character of the sandbank wave hydrodynamics. Severe wave breaking near the outer slope (see e.g. Fig. 19) and triad wave-wave interaction cause drastic spectral transformation across the sandbank. As high-frequency waves quickly dissipates within the first wave length low-frequency waves become increasingly important as wave propagates over the sandbank and wave energy is gradually shifted toward the infra-gravity band (see Fig. 20). Obviously, the spectral evolution toward low-frequency band increases as the water depth (R_c) over the sandbank decreases (see Annex B for details).

Figure 19 Severe wave breaking at the sandbank outer slope

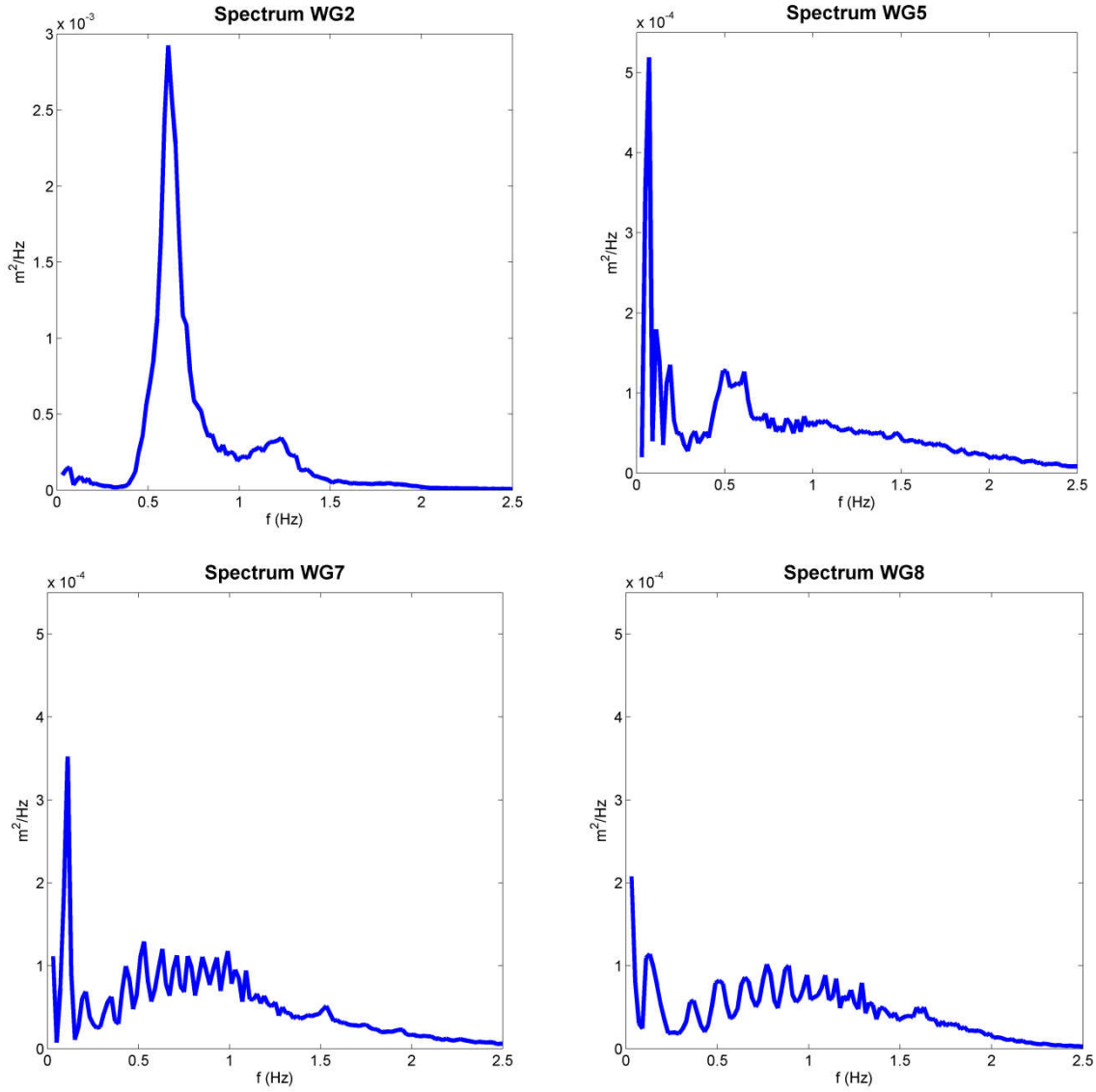

Figure 20 WP6-NOU-B7-R10-JSW3: Drastic spectral transformation across the sandbank: WG2, WG5, WG7, and WG8

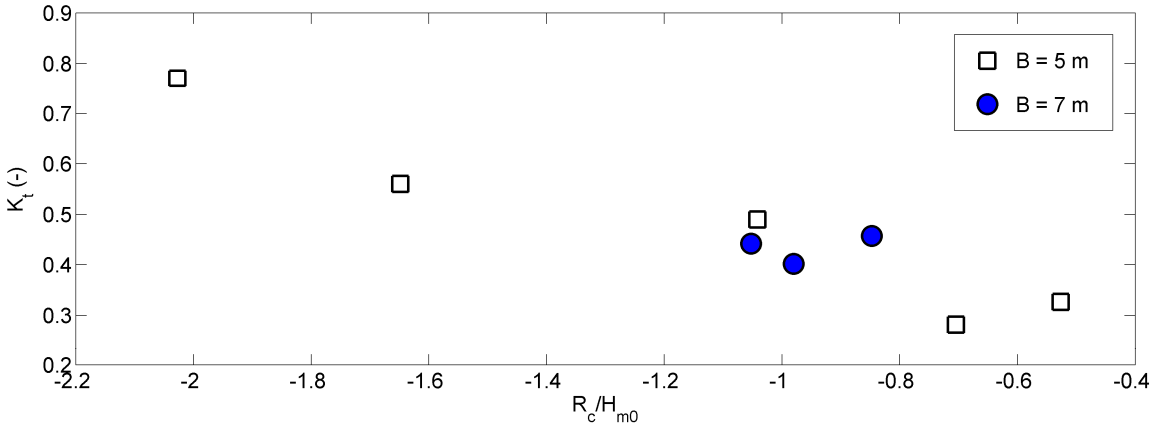

Figure 21 Effects of relative submergence and bank crest width

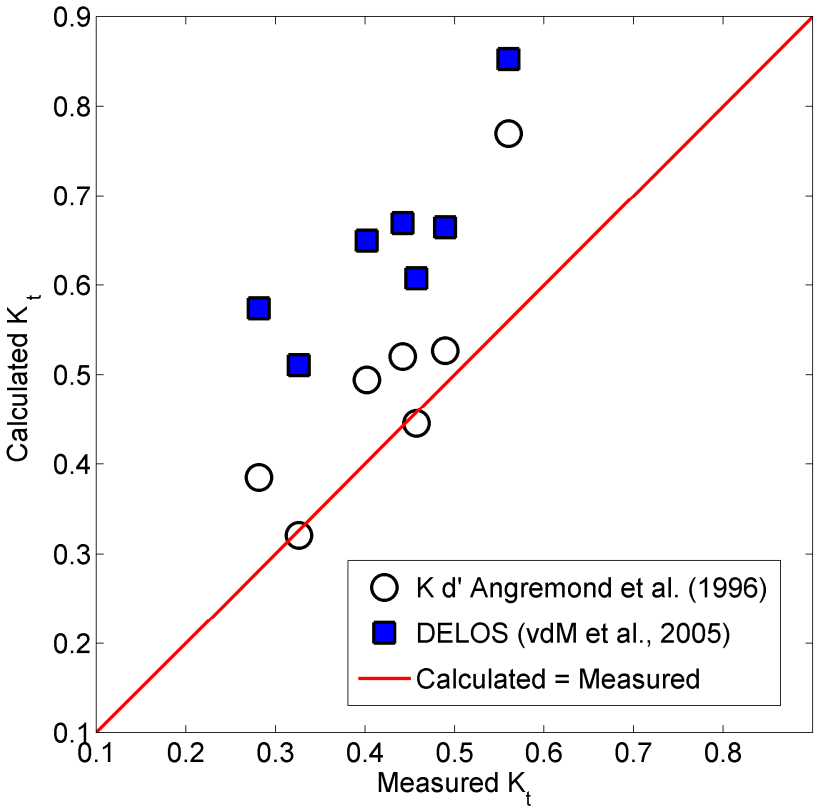

Figure 22 Experimental data of wave transmission at sandbanks in comparison with existing formulations of smooth and impermeable structures

Table 3 Measured wave heights across the sandbank

Test scenarios	WG2			Initial geometry				On-crest gauges H_{m0} (m)				WG8		K_t
	H_{m0} (m)	T_p (s)	$T_{m-1,0}$ (s)	B (m)	R_c (m)	R_c/H_{m0}	B/H_{m0}	WG3	WG5	WG6	WG7	H_{m0} (m)	$T_{m-1,0}$ (s)	(-)
WP6-NOU-B5-R05-JSW1	0.071	1.41	1.44	5	-0.05	-0.70	70.4					0.020	11.1	0.275
WP6-NOU-B5-R15-JSW1	0.074	1.41	1.42	5	-0.15	-2.03	67.6		0.062			0.057	1.52	0.770
WP6-NOU-B5-R05-JSW2	0.095	1.57	1.57	5	-0.05	-0.53	52.6					0.031	10.0	0.326
WP6-NOU-B5-R10-JSW2	0.096	1.57	1.55	5	-0.10	-1.04	52.1	0.074			0.045	0.047	2.05	0.490
WP6-NOU-B5-R15-JSW2	0.091	1.57	1.57	5	-0.15	-1.66	55.3		0.058		0.053	0.051	2.00	0.564
WP6-NOU-B7-R10-JSW2	0.095	1.57	1.54	7	-0.10	-1.05	73.7				0.044	0.042	1.81	0.442
WP6-NOU-B7-R10-JSW3	0.102	1.64	1.63	7	-0.10	-0.99	69.0		0.047		0.045	0.041	2.15	0.404
WP6-NOU-B7-R10-JSW4	0.118	1.70	1.70	7	-0.10	-0.85	59.3	0.085				0.054	3.23	0.458

Wave parameters are determined once the bank profile has become relatively stable (after approx. 1000 waves)
K_t is based on wave heights behind (WG8) and in front (WG2) of sandbank

For the functional design of the sandbank, it is important to evaluate the wave damping capacity of the sandbank. Table 3 summarizes the measured wave heights H_{m0} across the bank and the associated wave transmission coefficient. Note that wave parameters given in the table are determined once the bank profile has become relatively stable (after approximately 1000 waves). Unfortunately, due to the effect of high sediment concentration together with the shallow water depth over the crest, especially during passage of IG waves, the recorded signals from the on-crest wave gauges (WG3 through WG7) were mostly out-of-range.

Generally speaking, wide sandbanks are highly effective in damping waves. Figure 21 delineates the dependency of wave transmission on the major governing parameters. Similar to other type of structures, wave transmission over a wide sandbank addressed herein depends strongly on the relative submerged depth (R_c/H_{m0}) and somewhat weaker on the relative bank width (B/H_{m0} or B/L). However, Fig. 22 shows significant overestimations of wave transmission, in comparison with the experimental data, by the existing formulations of smooth and impermeable structures by Angremond et al. (1996) and DELOS (van der Meer et al., 2005). This can be explained by the fact that none of these formulations are valid for such a wide crest structure (B/H_{m0} ~ 50 - 70 or B/L ~ 2.0). The DELOS approach does not even account for the crest width and thus gives the largest discrepancy. More importantly, as mentioned earlier, most of the energy of short-period waves is dissipated within the first wave length or so and thus the energy behind the bank is largely of long-period waves. Therefore, it is generally insufficient to describe wave transmission over a wide sandbank in this case solely by short-period wave characteristics. For instance, inclusion of the spectral period $T_{m-1,0}$ (also given in Table 3), which gives more emphasis on the behaviour of waves in shallow water, should be considered.

Sandbank profile response

Besides the wave damping capacity, the extent of sandbank profile deformation to attack by cross-shore processes is an indicator of the nourishment efficiency.

Figures 22 through 30 show the time-dependent bank profile response for each of the test scenarios, respectively. It is generally observed that major bank deformation took place within the first 1000 waves, after which the bank profile was relatively stable with a slow evolution rate. Profile changes mostly occurred on the outer bank slope with the typical storm-induced erosion-accretion pattern, the inner slope remained relatively intact. In cases of low crest submergence, i.e. $-R_c/H_{m0} < 1.0$, the bank crest was even slightly elevated due to onshore transport and deposition (see e.g. Figs. 23 and 25).

Within the tested conditions, it appears that the sandbank did not undergo major profile deformation. There was no clear difference in the extent of profile deformation between the two cases of bank crest width. The overall dimensions of the sandbank were more or less unchanged during wave attacks, which helped maintain wave transmission as it was initially designed.

c. Summary and Remarks on large-scale nourishment

Eight mobile-bed experiments on the large-scale nourishment by sandbanks were carried out to increase understanding of the physical processes involved. The test program covers several typical monsoon wave and sandbank geometric conditions.

The wave hydrodynamics at the sandbank is typically governed by drastic spectral transformation through the processes of dissipation of short-period waves and generation of IG waves. Because short-period energy is mostly dissipated within a distance less than the bank crest width, long-period energy is dominant in the transmitted wave spectra behind the bank. The wide sandbank appears to generally effective in damping waves with small relative crest submergence (i.e. $-R_c/H_{m0} < 1.0$). None of the existing formulations of wave transmission at conventional structures are reliable for such a wide sandbank crest and more importantly as the effect of IG waves is not included. For the functional design on wave transmission, the approach by Angremond et al. (1996) for smooth and impermeable structures can be used as a first approximation. For more reliable prediction of wave transmission an appropriate numerical model validated with the experimental data can be used.

Generally speaking, the sandbank profile response to the cross-shore attack by monsoon waves appears to be rather mild, even in cases of small crest submergence. It can be concluded that the cross-shore processes are generally important for consideration of the sandbank wave damping capacity rather than that of the design nourishment volume. The weak and slow profile deformation together with high wave damping capacity also suggest that the nourishment by near-shore sandbanks can be a viable solution.

Before coming up with a design for the nourishment, extensive numerical morphological studies are necessary to incorporate some important effects such as 3D bathymetry, long-shore transport processes, spatial layout, etc. Experimental data on the wave hydrodynamics and profile evolution should be used for numerical validations.

WP6-NOU-B5-R05-JSW1

R_c/H_{m0} = –0.70

B/H_{m0} = 70.4

K_t = 0.275

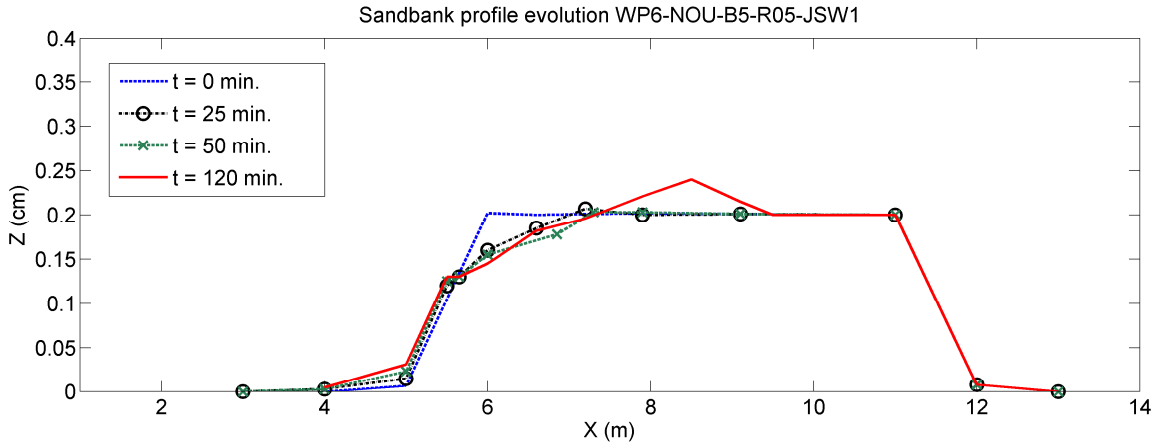

Figure 23 Sandbank profile response - Scenario WP6-NOU-B5-R05-JSW1

WP6-NOU-B5-R15-JSW1

R_c/H_{m0} = –2.03

B/H_{m0} = 67.6

K_t = 0.77

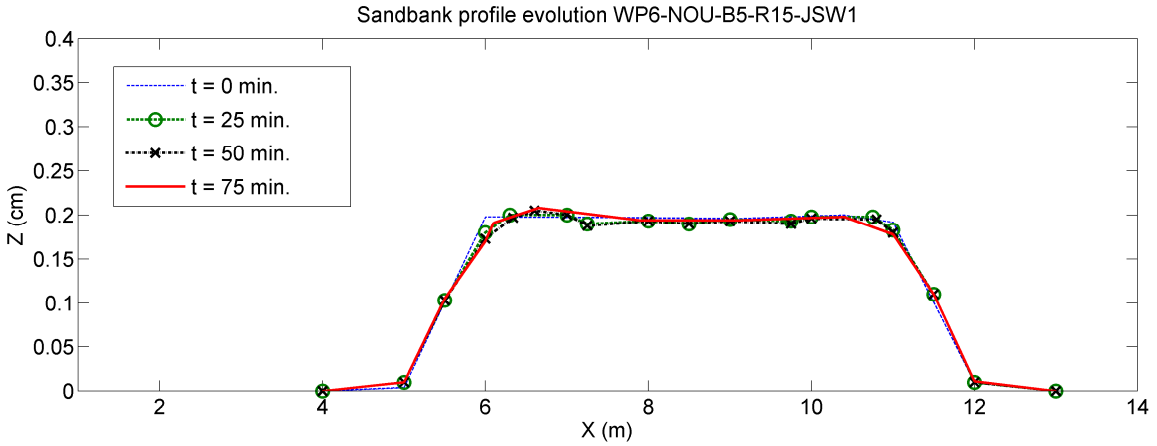

Figure 24 Sandbank profile response - Scenario WP6-NOU-B5-R15-JSW1

WP6-NOU-B5-R05-JSW2

R_c/H_{m0} = −0.53

B/H_{m0} = 52.6

K_t = 0.326

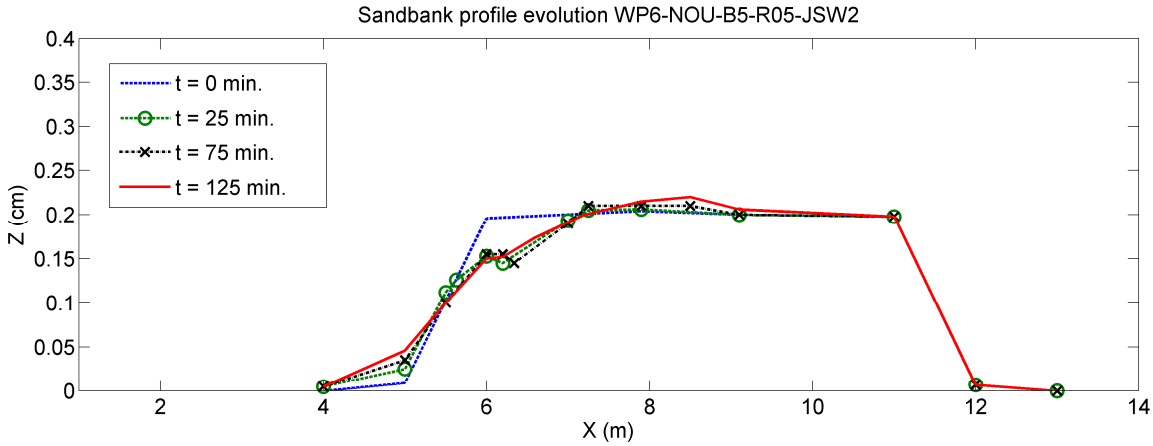

Figure 25 Sandbank profile response - Scenario WP6-NOU-B5-R05-JSW2

WP6-NOU-B5-R10-JSW2

R_c/H_{m0} = −1.04

B/H_{m0} = 52.1

K_t = 0.49

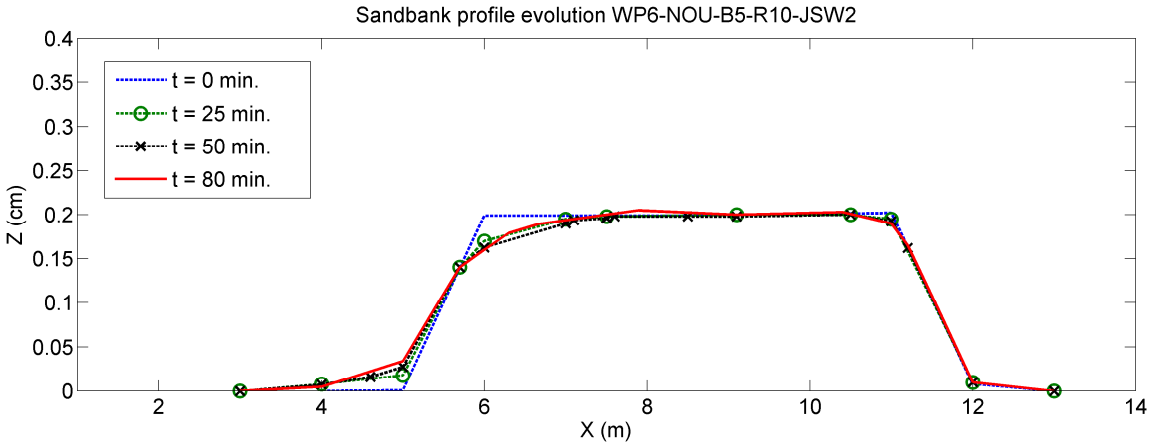

Figure 26 Sandbank profile response - Scenario WP6-NOU-B5-R10-JSW2

WP6-NOU-B5-R15-JSW2

$R_c/H_{m0} = -1.66$

$B/H_{m0} = 55.2$

$K_t = 0.564$

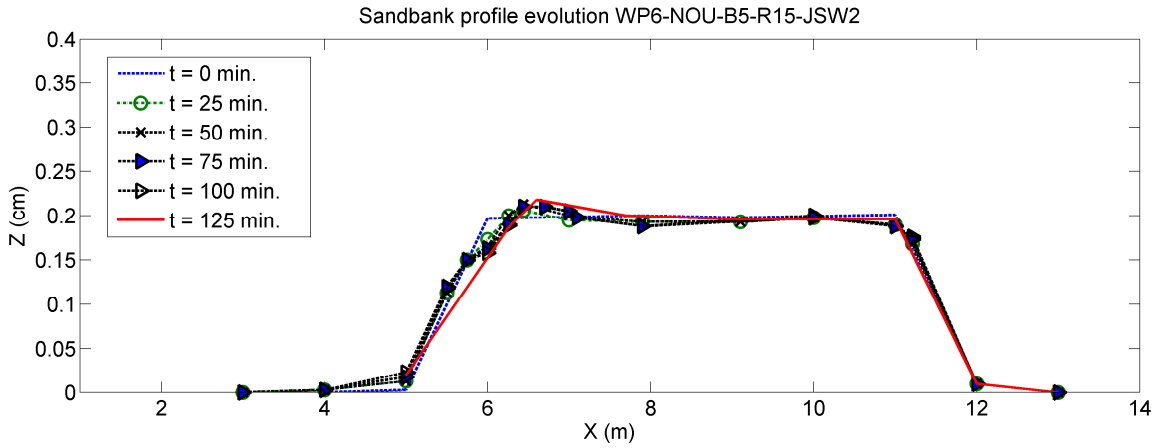

Figure 27 Sandbank profile response - Scenario WP6-NOU-B5-R15-JSW2

WP6-NOU-B7-R10-JSW2

$R_c/H_{m0} = -1.05$

$B/H_{m0} = 73.7$

$K_t = 0.442$

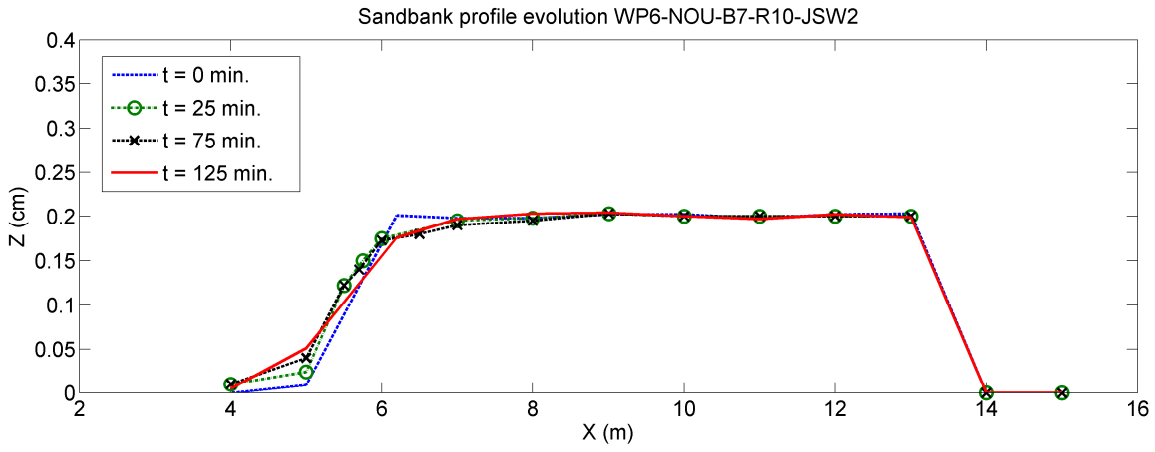

Figure 28 Sandbank profile response - Scenario WP6-NOU-B7-R10-JSW2

WP6-NOU-B7-R10-JSW3

R_c/H_{m0} = –0.99

B/H_{m0} = 69.0

K_t = 0.404

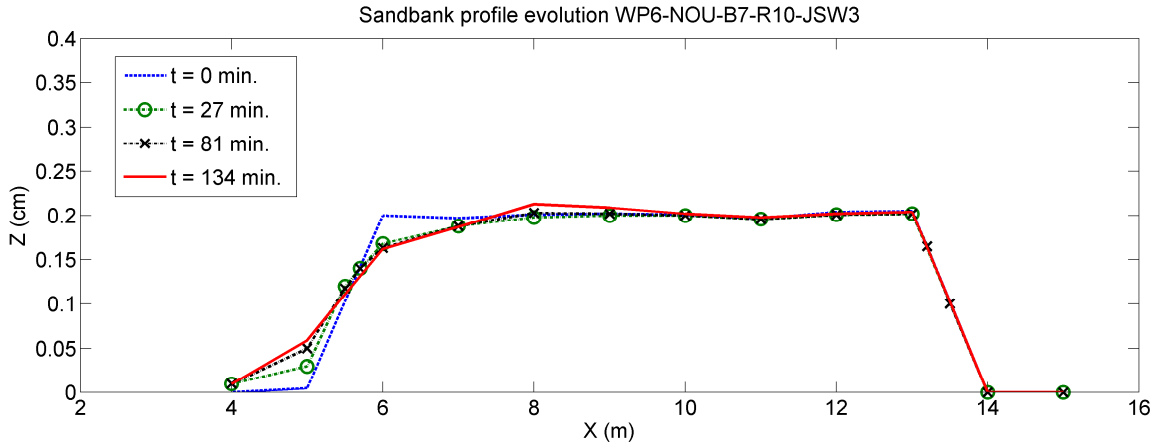

Figure 29 Sandbank profile response - Scenario WP6-NOU-B7-R10-JSW3

WP6-NOU-B7-R10-JSW4

R_c/H_{m0} = –0.85

B/H_{m0} = 59.3

K_t = 0.458

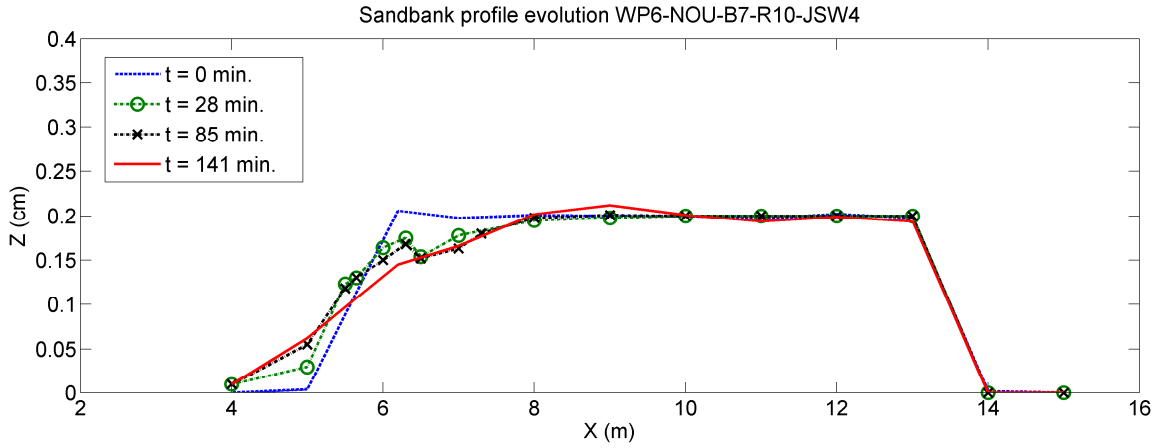

Figure 30 Sandbank profile response - Scenario WP6-NOU-B7-R10-JSW4

REFERENCES

Angremond, K., Van der Meer, J.W. and de Jong, R.J., 1996. Wave transmission at low-crested structures. Proc. 25th ICCE, ASCE, Orlando, USA.

Baldock, T. E., 2012. Dissipation of incident forced long waves in the surf zone – Implications for the concept of "bound" wave release at short wave breaking. Coastal Engineering, 60, pp. 276-285.

Đặng Thị Linh và Thiều Quang Tuấn, 2015. Xây dựng quan hệ chu kỳ và chiều cao của sóng gió cho mùa vùng biển Bắc và Bắc Trung Bộ nước ta. *Hội nghị khoa học thường niên năm 2015, Đại học Thủy lợi*, Hà Nội, 407 – 409.

Horstman, E., Dohmen-Janssen, M., Narra, P., van den Berg, NJ., Siemerink, M., Balke, T., Bouma, T., and Hulscher, S., 2012. Wave attenuation in mangrove forests; field data obtained in Trang, Thailand. *Proc. 33nd Int. Conf. Coastal Eng.*, ASCE , pp. 40.

Hughes, A.S., 1993. Physical models and laboratory techniques in coastal engineering, *World Scientific, Singapore*, 568 pp.

Phan, L.K., van Thiel de Vries, J.S.M., and Stive, M.J.F., 2014. Coastal mangrove squeeze in the Mekong Delta. Journal of Coastal Research, 31, 2, pp. 233 – 243.

Tuan, T.Q., Tien, N.V. and Verhagen, H.J., 2016. Wave transmission over submerged, smooth and impermeable breakwaters on a gentle and shallow foreshore. In: Proc. 9th PIANC-COPEDEC, pp. 897-905, Rio de Janeiro, BRAZIL.

Van der Meer, J.W., Daemen, I.F.R., 1994. Stability and wave transmission at low crested rubble mound structures. Journal of Waterway, Port Coastal and Ocean Engineering, 1, 1-19.

Van der Meer, J. W., Briganti, R., Zanuttigh, B. and Wang, B., 2005. Wave transmission and reflection at low-crested structures: Design formulae, oblique wave attack and spectral change. Coastal Engineering, 52, 915 - 929.

Zelt, J.A. and Skjelbreia, J.E., 1992. Estimating incident and reflected wave fields using an arbitrary number of wave gauges. *Proc. 23rd Int. Conf. Coastal Eng.*, ASCE, pp. 777-789.

ANNEX A Experimental data of wave transmission at porous breakwaters

	Test	Depth D (m)	Freeboard Rc (m)	Reflection R (-)	Hm0 (m)			Tp (s)	Tm-1,0 (s)	
					WGin	WG6	WG7		WG6	WG7
1	WP6-BW-JSW1-D0-20	0.20	0.20	0.133	0.090	0.093	0.089	1.73	2.37	2.63
2	WP6-BW-JSW2-D0-20	0.20	0.20	0.124	0.111	0.104	0.099	1.82	2.40	2.59
3	WP6-BW-JSW3-D0-20	0.20	0.20	0.124	0.138	0.107	0.102	1.94	2.44	2.67
4	WP6-BW-JSW4-D0-20	0.20	0.20	0.120	0.154	0.113	0.105	2.00	2.59	2.75
5	WP6-BW-JSW5-D0-20	0.20	0.20	0.128	0.175	0.115	0.105	2.10	3.01	3.29
6	WP6-BW-JSW6-D0-20	0.20	0.20	0.131	0.195	0.117	0.105	2.14	3.23	3.51
7	WP6-BW-JSW1-D0-30	0.30	0.10	0.097	0.088	0.095	0.094	1.74	2.12	2.26
8	WP6-BW-JSW2-D0-30	0.30	0.10	0.106	0.104	0.116	0.114	1.82	2.50	2.74
9	WP6-BW-JSW3-D0-30	0.30	0.10	0.098	0.138	0.136	0.131	1.94	2.57	2.75
10	WP6-BW-JSW4-D0-30	0.30	0.10	0.105	0.154	0.144	0.139	2.00	2.54	2.73
11	WP6-BW-JSW5-D0-30	0.30	0.10	0.110	0.182	0.156	0.149	2.10	2.57	2.95

	Test	Depth D (m)	Freeboard Rc (m)	Reflection R (-)	Hm0 (m)			Tp (s)	Tm-1,0 (s)	
					WGin	WG6	WG7		WG6	WG7
12	WP6-BW-JSW6-D0-30	0.30	0.10	0.117	0.197	0.160	0.150	2.14	2.62	3.11
13	WP6-BW-JSW1-D0-40	0.40	0.00	0.116	0.091	0.095	0.094	1.74	1.94	1.99
14	WP6-BW-JSW2-D0-40	0.40	0.00	0.113	0.110	0.117	0.115	1.82	2.11	2.22
15	WP6-BW-JSW3-D0-40	0.40	0.00	0.117	0.133	0.144	0.143	1.94	2.31	2.61
16	WP6-BW-JSW4-D0-40	0.40	0.00	0.121	0.158	0.165	0.162	2.00	2.58	2.93
17	WP6-BW-JSW5-D0-40	0.40	0.00	0.122	0.181	0.187	0.179	2.10	2.83	3.15
18	WP6-BW-JSW6-D0-40	0.40	0.00	0.128	0.196	0.194	0.185	2.14	2.87	3.12
19	WP6-BW-JSW1-D0-50	0.50	-0.10	0.154	0.092	0.094	0.093	1.74	1.74	1.85
20	WP6-BW-JSW2-D0-50	0.50	-0.10	0.152	0.110	0.114	0.113	1.82	1.91	2.08
21	WP6-BW-JSW3-D0-50	0.50	-0.10	0.152	0.136	0.144	0.141	1.94	2.27	2.42
22	WP6-BW-JSW4-D0-50	0.50	-0.10	0.155	0.155	0.162	0.161	2.00	2.41	2.57
23	WP6-BW-JSW5-D0-50	0.50	-0.10	0.161	0.183	0.192	0.188	2.10	2.52	2.69

	Test	Depth D (m)	Freeboard Rc (m)	Reflection R (-)	Hm0 (m)			Tp (s)	Tm-1,0 (s)	
					WGin	WG6	WG7		WG6	WG7
24	WP6-BW-JSW6-D0-50	0.50	-0.10	0.164	0.198	0.206	0.200	2.14	2.57	2.76
25	WP6-BW-JSW1-D0-55	0.55	-0.15	0.105	0.093	0.092	0.092	1.74	1.72	1.80
26	WP6-BW-JSW2-D0-55	0.55	-0.15	0.119	0.113	0.113	0.112	1.82	1.88	1.98
27	WP6-BW-JSW3-D0-55	0.55	-0.15	0.118	0.140	0.142	0.141	1.94	2.10	2.18
28	WP6-BW-JSW4-D0-55	0.55	-0.15	0.133	0.158	0.161	0.159	2.00	2.21	2.30
29	WP6-BW-JSW5-D0-55	0.55	-0.15	0.141	0.185	0.188	0.187	2.10	2.34	2.48
30	WP6-BW-JSW6-D0-55	0.55	-0.15	0.139	0.200	0.205	0.202	2.14	2.42	2.58
31	WP6-BW-JSW1-D0-20	0.20	0.20	0.433	0.091	0.101	0.026	1.73	2.07	5.10
32	WP6-BW-JSW2-D0-20	0.20	0.20	0.392	0.109	0.117	0.029	1.82	2.08	4.81
33	WP6-BW-JSW3-D0-20	0.20	0.20	0.330	0.135	0.132	0.029	1.94	2.21	5.03
34	WP6-BW-JSW4-D0-20	0.20	0.20	0.298	0.152	0.134	0.032	2.00	2.42	6.05
35	WP6-BW-JSW5-D0-20	0.20	0.20	0.257	0.176	0.139	0.034	2.10	2.88	8.22

	Test	Depth D (m)	Freeboard Rc (m)	Reflection R (-)	Hm0 (m)			Tp (s)	Tm-1,0 (s)	
					WGin	WG6	WG7		WG6	WG7
36	WP6-BW-JSW6-D0-20	0.20	0.20	0.247	0.189	0.136	0.035	2.14	3.22	8.53
37	WP6-BW-JSW1-D0-30	0.30	0.10	0.494	0.092	0.118	0.039	1.73	1.96	2.55
38	WP6-BW-JSW2-D0-30	0.30	0.10	0.500	0.108	0.151	0.044	1.82	2.12	3.46
39	WP6-BW-JSW3-D0-30	0.30	0.10	0.453	0.135	0.173	0.053	1.94	2.23	3.40
40	WP6-BW-JSW4-D0-30	0.30	0.10	0.421	0.153	0.184	0.057	2.00	2.26	3.36
41	WP6-BW-JSW5-D0-30	0.30	0.10	0.378	0.184	0.192	0.064	2.10	2.44	3.84
42	WP6-BW-JSW6-D0-30	0.30	0.10	0.365	0.188	0.194	0.068	2.14	2.54	3.85
43	WP6-BW-JSW1-D0-40	0.40	0.00	0.397	0.092	0.117	0.054	1.79	1.84	2.05
44	WP6-BW-JSW2-D0-40	0.40	0.00	0.402	0.112	0.145	0.067	1.82	1.95	2.18
45	WP6-BW-JSW3-D0-40	0.40	0.00	0.396	0.136	0.175	0.085	1.94	2.14	2.81
46	WP6-BW-JSW4-D0-40	0.40	0.00	0.392	0.153	0.189	0.097	2.00	2.28	3.12
47	WP6-BW-JSW5-D0-40	0.40	0.00	0.367	0.182	0.206	0.110	2.10	2.57	3.45

	Test	Depth D (m)	Freeboard Rc (m)	Reflection R (-)	Hm0 (m)			Tp (s)	Tm-1,0 (s)	
					WGin	WG6	WG7		WG6	WG7
48	WP6-BW-JSW6-D0-40	0.40	0.00	0.348	0.195	0.212	0.116	2.14	2.64	3.38
49	WP6-BW-JSW1-D0-50	0.50	-0.10	0.258	0.092	0.105	0.072	1.73	1.75	1.71
50	WP6-BW-JSW2-D0-50	0.50	-0.10	0.274	0.111	0.127	0.084	1.82	1.89	1.88
51	WP6-BW-JSW3-D0-50	0.50	-0.10	0.301	0.135	0.156	0.104	1.94	2.19	2.23
52	WP6-BW-JSW4-D0-50	0.50	-0.10	0.305	0.153	0.173	0.115	2.00	2.34	2.36
53	WP6-BW-JSW5-D0-50	0.50	-0.10	0.310	0.180	0.196	0.132	2.10	2.52	2.45
54	WP6-BW-JSW6-D0-50	0.50	-0.10	0.319	0.195	0.207	0.138	2.14	2.61	2.57
55	WP6-BW-JSW1-D0-55	0.55	-0.15	0.211	0.093	0.101	0.076	1.73	1.70	1.69
56	WP6-BW-JSW2-D0-55	0.55	-0.15	0.229	0.111	0.121	0.090	1.82	1.84	1.87
57	WP6-BW-JSW3-D0-55	0.55	-0.15	0.238	0.139	0.148	0.109	1.94	2.06	2.06
58	WP6-BW-JSW4-D0-55	0.55	-0.15	0.249	0.157	0.164	0.122	2.00	2.21	2.16
59	WP6-BW-JSW5-D0-55	0.55	-0.15	0.256	0.181	0.184	0.142	2.10	2.36	2.31
60	WP6-BW-JSW6-D0-55	0.55	-0.15	0.262	0.196	0.198	0.150	2.14	2.51	2.44

ANNEX B Measured wave spectral transformation across the sandbank

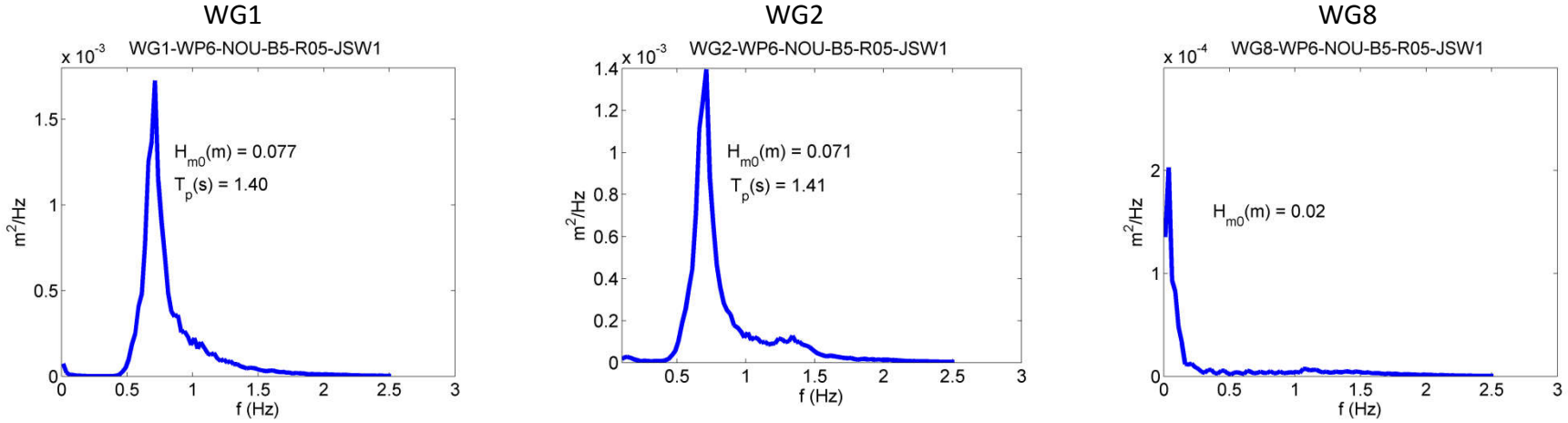

Fig. B1 Measured wave spectra WP6-NOU-B5-R05-JSW1

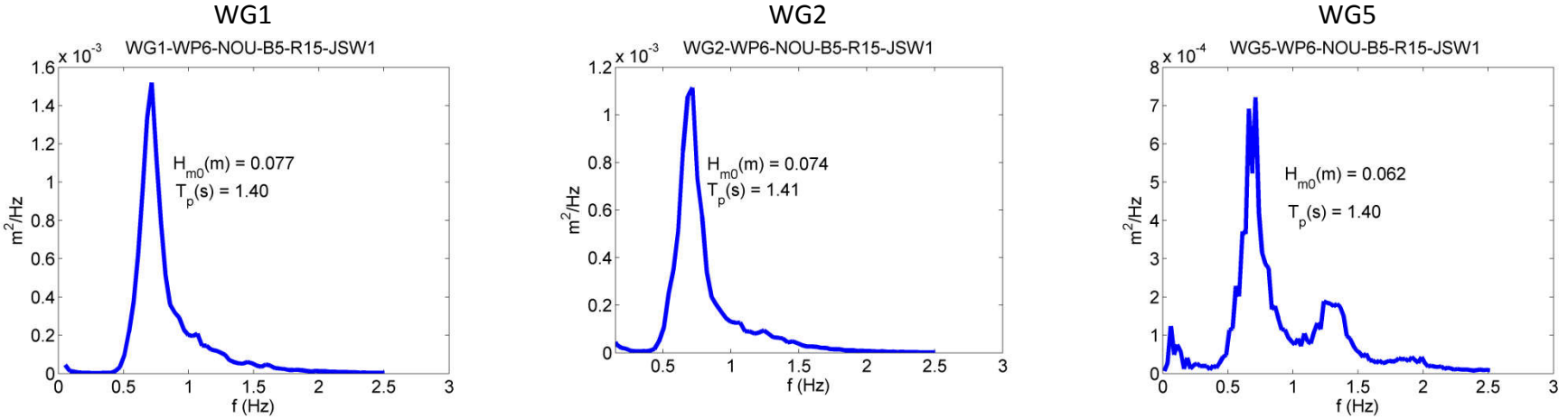

Fig. B2 Measured wave spectra WP6-NOU-B5-R15-JSW1

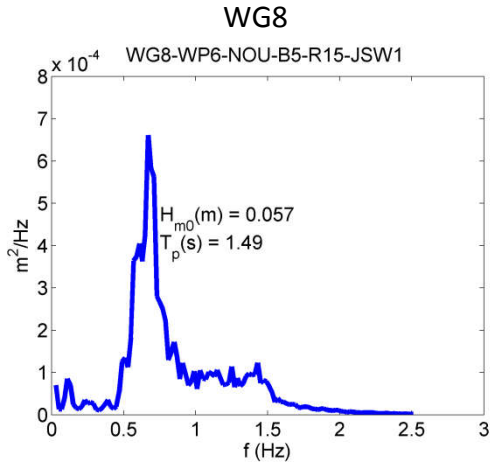

Fig. B2 Measured wave spectra WP6-NOU-B5-R15-JSW1 (continued)

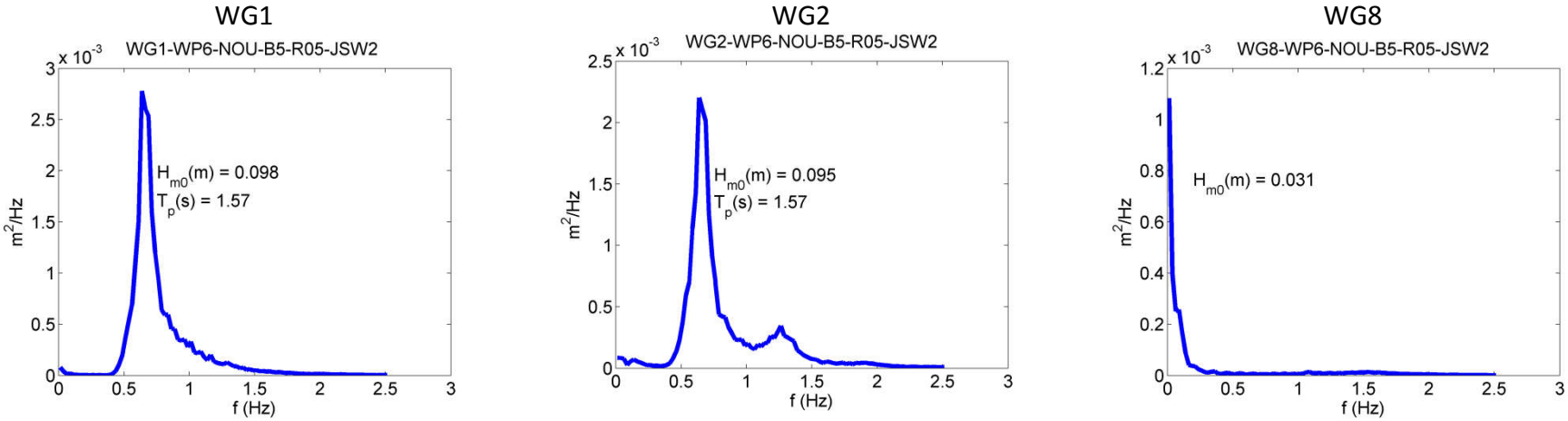

Fig. B3 Measured wave spectra WP6-NOU-B5-R05-JSW2

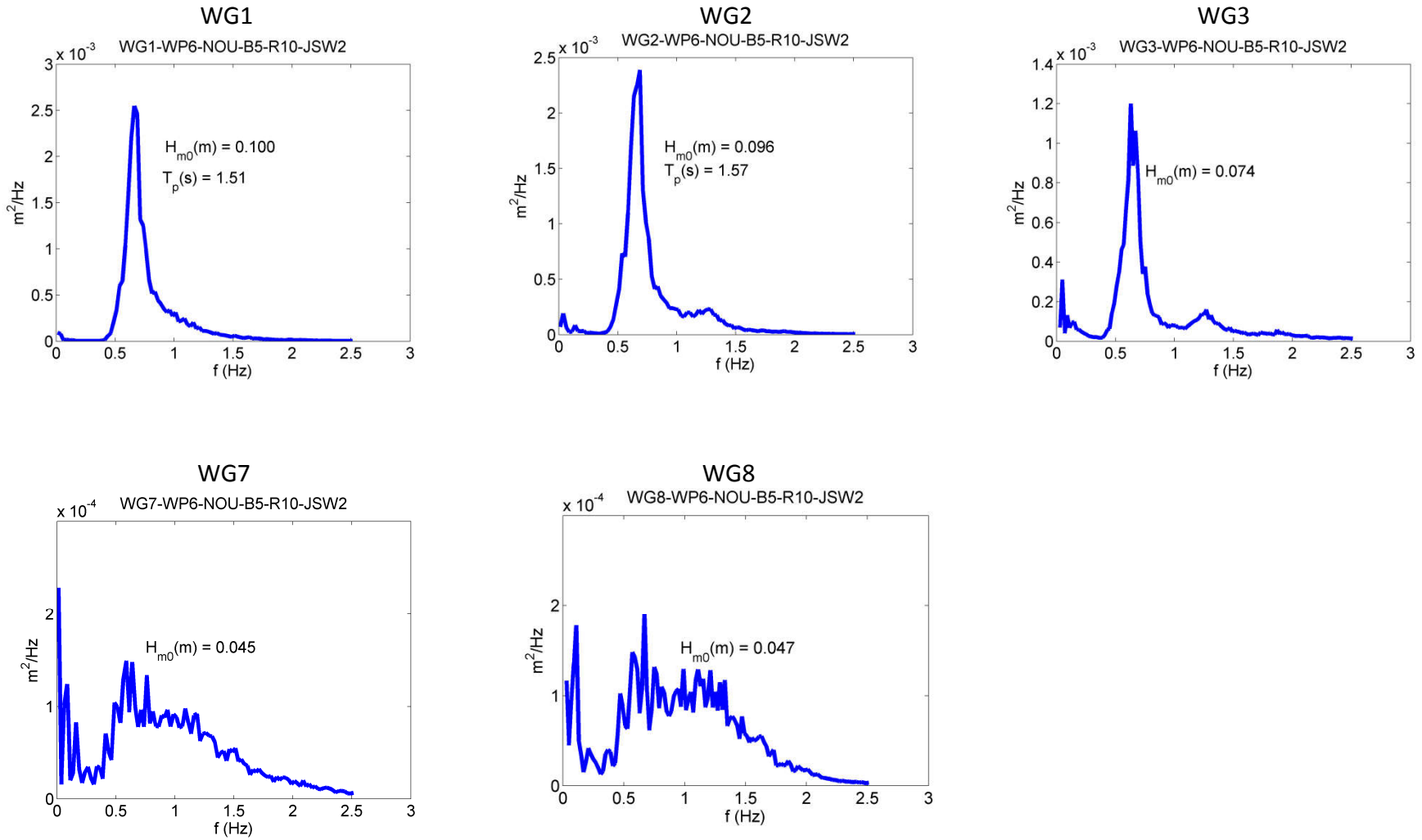

Fig. B4 Measured wave spectra WP6-NOU-B5-R10-JSW2

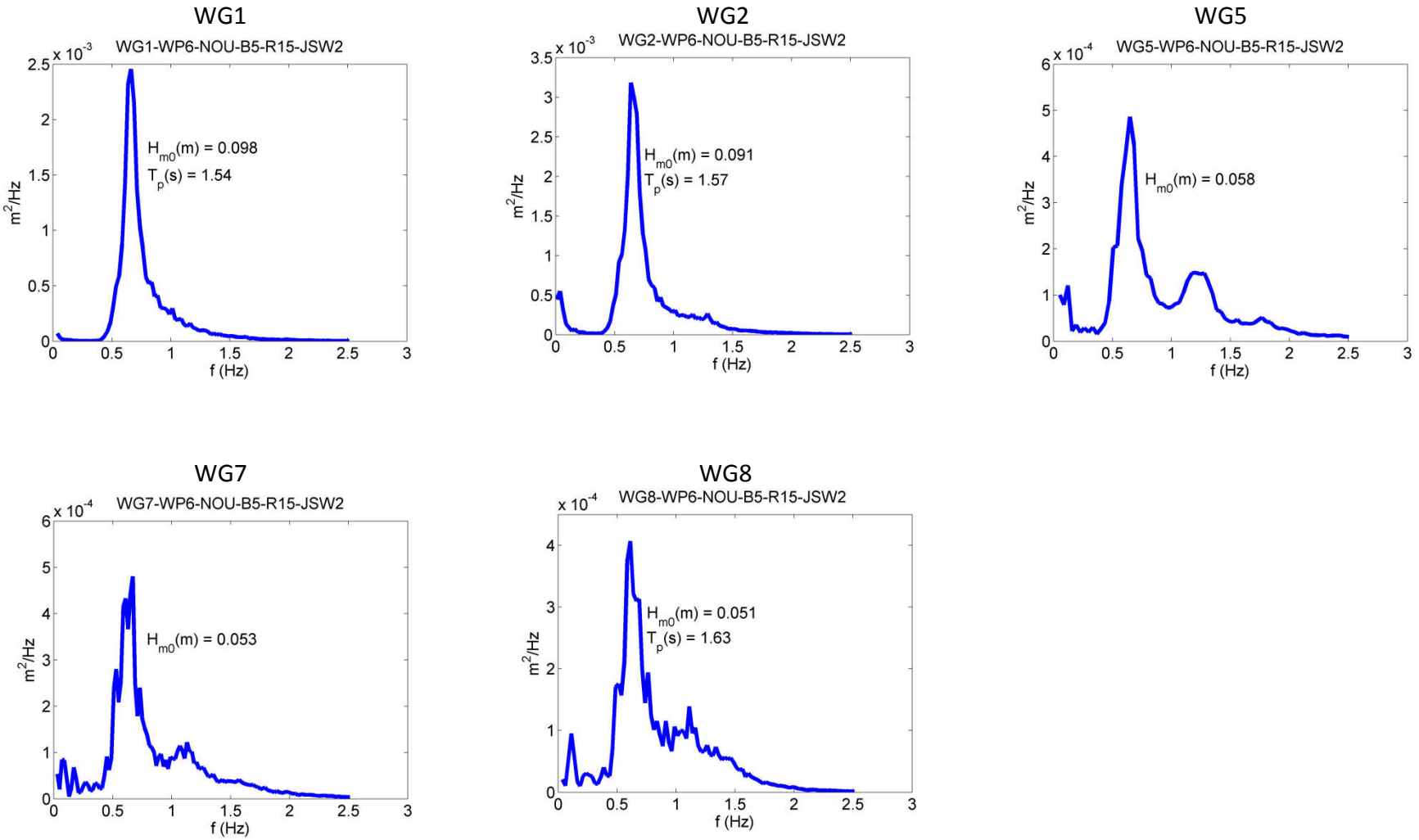

Fig. B5 Measured wave spectra WP6-NOU-B5-R15-JSW2

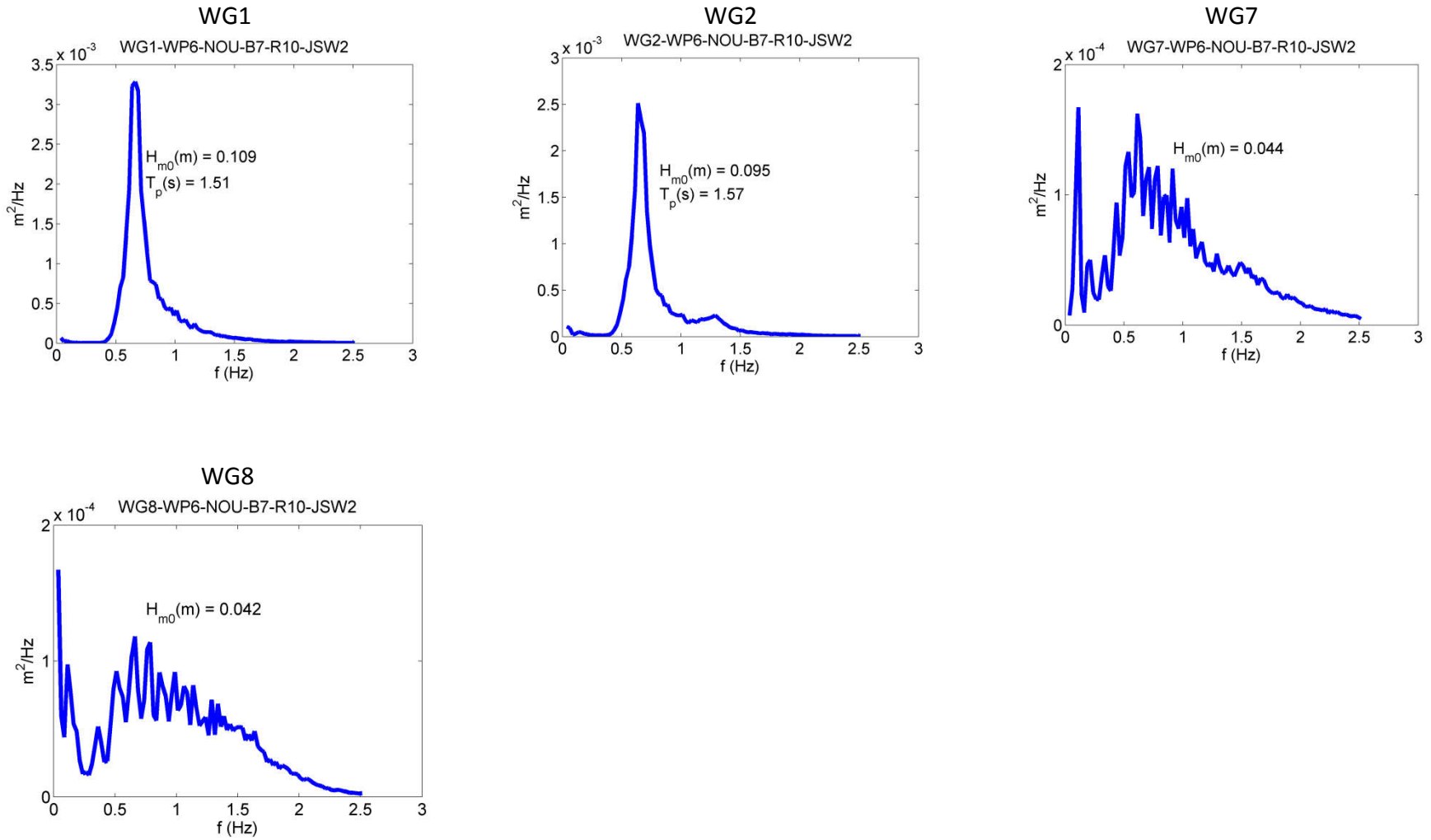

Fig. B6 Measured wave spectra WP6-NOU-B7-R10-JSW2

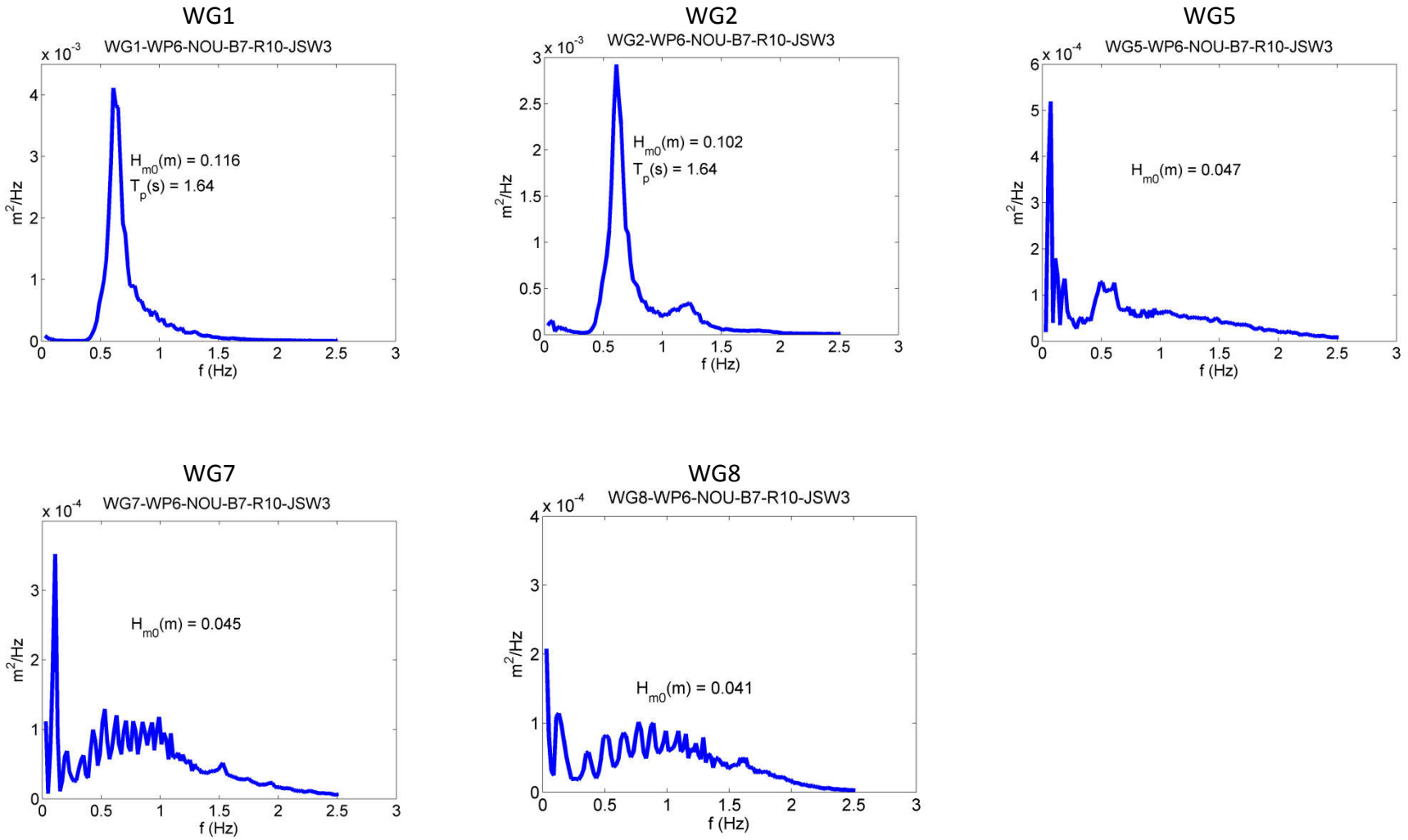

Fig. B7 Measured wave spectra WP6-NOU-B7-R10-JSW3

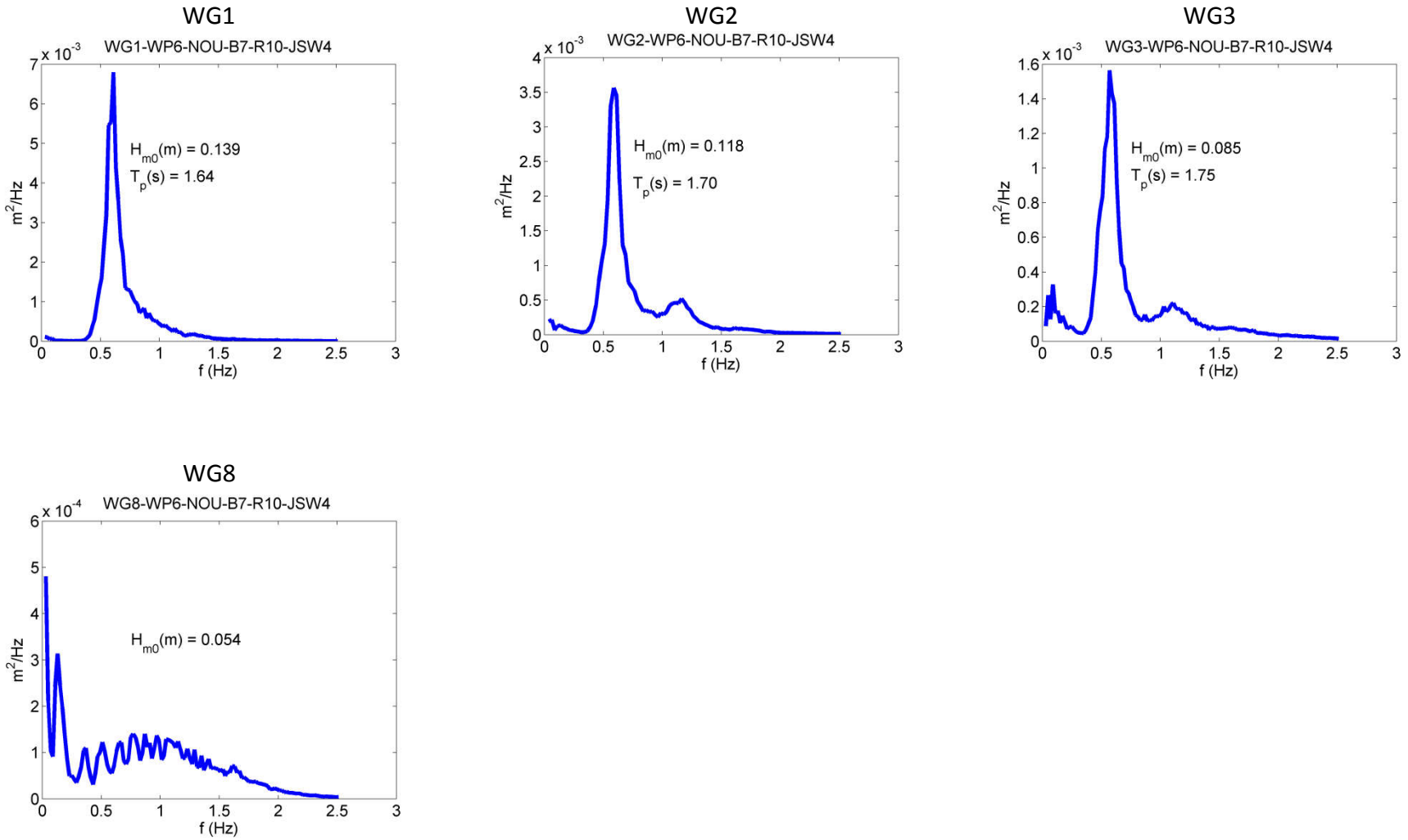

Fig. B8 Measured wave spectra WP6-NOU-B7-R10-JSW4